Original Article

Comparative Study of The Therapeutic Potential of Bone Marrow-derived Mesenchymal Stem Cells Versus Their Secreted Vesicles on Renal Corpuscles of Rats with Diabetic Nephropathy: A Histological, Biochemical and Morphometric Study

Eman Magdy Moussa, Inaam Philipa Philip Kelada, Safinaz H. Safwat and Silvia Kamil Seddik Sawires

Department of Histology and Cell Biology, Faculty of Medicine, Alexandria University, Egypt

ABSTRACT

Introduction: Diabetic nephropathy (DN) is one of the most prevalent microvascular consequences of diabetes that results in end-stage renal disease. Bone marrow - mesenchymal stem cells (BM-MSCs) and their secreted extracellular vesicles (EVs) become prospective treatment approaches for DN.

Aim of the Work: To compare the therapeutic potential of BM-MSCs and EVs on induced diabetic nephropathy in rats.

Materials and Methods: Four young male albino rats were utilized for isolation of BM-MSCs and EVs. Forty-two adult male albino rats were divided as follow: Group I (Control group): 18 rats. Group II (treated group): 24 rats, each administered an intraperitoneal streptozotocin injection (STZ) once (55 mg/kg body weight). After proved being diabetic (blood glucose > 250 mg/dl), they were further subdivided equally into: subgroup IIA (DN subgroup), subgroup IIB (spontaneous recovery subgroup), subgroup IIC (DN + BM-MSCs) and subgroup IID (DN + EVs). At the end of the research, blood and urine samples were taken for biochemical evaluation. For light, electron, and histo-morphometric investigations, the kidneys were removed and processed. The collected data underwent statistical analysis.

Results: Histological examination of DN subgroup revealed irregular thickened glomerular basement membrane (GBM), detached apoptotic endothelial cells, vacuolated parietal cells, effacement of the secondary processes of podocytes, inflammatory cells infiltration, mesangial cell proliferation and mesangial matrix expansion. These findings were confirmed biochemically by significant increase of kidney parameters, oxidative and inflammatory markers with significant decrease of antioxidant markers. Morphometric studies showed significant increase of GBM thickness and area percentage of collagen fibers. Treatment with BM-MSCs alleviated renal corpuscles histological changes and improved biochemical markers and morphometric analysis induced by diabetes. The administration of EVs revealed better results.

Conclusion: MSCs and EVs could be quite beneficial for treating DN. However, EVs have promising therapeutic modality over transplanted BM-MSCs with fewer side effects.

INTRODUCTION

Diabetes mellitus (DM) is a worldwide pandemic health issue that is estimated to affect 700 million people in 2045 on the basis of the latest International Diabetes Federation report[1]. Persistent hyperglycemic status induce mitochondria to generate a lot of reactive oxygen species (ROS), resulting in oxidative stress in cells[2], inflammation, increased advanced-glycation end-products (AGEs) and hence, grave micro- and macrovascular problems[3,4]. The most severe microvascular issue associated with DM is diabetic nephropathy (DN) which is assumed to be the main factor contributing to end-stage renal disease. (ESRD)[5]. DN is a chronic, advanced multifactorial disorder affecting about 45% of type I DM and type II DM patients and increasing their morbidity and mortality[6]. The traditional drug therapy of DN mostly couldn't prevent the development of ESRD that necessitates renal replacement therapy as dialysis and kidney transplantation[7]. Dialysis could adversely affect the patient's quality of life and represents an economic burden[8]. Meanwhile, for patients with ESRD, kidney transplantation is the only viable treatment. Nevertheless, scarcity of organ donors and potential organ rejection limit its application[9]. Therefore, exploring new therapeutic strategy to treat or prevent this highly destructive condition and improve patients' survival and quality of life is mandatory.

Regenerative medicine is a novel emerging medical arena that aims to improve or replace the damaged tissues and restore their normal function. Stem cell-based technology or their secreted extracellular vesicles are emerged to be a potentially beneficial technique in this biomedicine field[10].

Mesenchymal stem cells (MSCs) have been a significant research topic among the numerous varieties of stem cells due to their special qualities like self-renewal

capability, pluripotency, intrinsic homing ability and low immunogenicity[11]. Transplantation of bone marrow mesenchymal stem cells (BM-MSCs) has been widely employed in studies for cardiovascular, immunological, and neurological illnesses, with promising outcomes[12,13]. It possesses immunomodulatory, anti-apoptotic, anti-fibrotic, angiogenic and anti-inflammatory properties granting their therapeutic potentials[14,15].

Recently, extracellular vesicles (EVs), a new promising therapeutic modality, have attracted a lot of interest due to their parts in cell-to-cell communication, immunomodulation and angiogenesis[16]. EVs are naturally occurring nanoparticles released from all cells into their environment[17]. They are lipid-bilayer vesicles containing lipids, proteins and various nucleic acids that are essential in maintaining cellular homeostasis. They can be extracted in *vitro* from cell-conditioned medium as well as from various bodily fluids such plasma, saliva, urine, semen, and breast milk[18]. They can be categorized into three types: microvesicles, exosomes and apoptotic bodies. Surface-expressed ligands help EVs engage with target cells[19]. Extracellular vesicles (EVs) decreased the extent of the infarct in a rat model of acute myocardial infarction when given systemically[20]. Following a stroke, MSC-EVs may have a neuroprotective impact[21]. They reduced pulmonary inflammation in acute lung damage models and aided liver regeneration in drug-induced liver damage models[22,23]. Their potential benefits have been credited with their anti-inflammatory and anti-fibrotic properties, implying that MSCs-EVs may offer a unique therapeutic option for diseases[24].

The purpose of this study was to evaluate the renal corpuscle's histological alterations in adult male albino rats after STZ-induced diabetes. Furthermore, comparing the therapeutic potential of BM-MSCs versus their EVs in improving streptozotocin induced diabetic nephropathy.

MATERIALS AND METHODS

Chemicals

Streptozotocin was obtained from Sigma, Aldrich (St. Louis, MO, USA).

Citrate buffer was made by Biochemistry Department, Faculty of Medicine, Alexandria University.

In-vitro methods

In-*vitro* study was performed at the Center of Excellence for Research in Regenerative Medicine and its Applications (CERRMA), Faculty of Medicine, Alexandria University.

Isolation of BM-MSCs[25,26]

Four albino rats (weighing 27-33 g, aged 2 weeks) purchased from the Animal House of Physiology Department, Faculty of Medicine, Alexandria University were sacrificed using overdose of chloroform anesthesia. Under a vertical laminar air-flow hood with an aseptic technique, the femurs with the surrounding muscular

tissues were obtained bilaterally, soaked in 70% ethanol for 2 minutes for disinfection, then the muscles were scraped off and phosphate buffer saline (PBS) (Biowest, USA) was used to wash the bones.

After that, both ends of the femur were cut and flushed the marrow cavity with complete culture media (CCM) repeatedly to obtain bone marrow cell suspension. CCM was prepared by use of low glucose Dulbecco's Modified Eagle's Medium (LG-DMEM, Lonza, Switzerland) combined with 10% Fetal Bovine Serum (FBS, Hyclone, Logan, UT, USA), 1% L-glutamine, and 1% Penicillin/Streptomycin (Lonza, Switzerland). Then, the bone spicules and clumps were removed from the bone marrow cell suspension by filtering it through a 70 µm filter mesh before centrifuging it at 1000 x g for five minutes. The formed cell pellets were re-suspended in CCM, conveyed into t-25 cm^2 flasks and incubated in CO2 incubator in a humidified atmosphere at 37oC and 5% CO_2. After 48 hours of culture, the culture media was changed to eliminate non-adherent hematopoietic cells, and it was then changed once every two to three days to feed the cells until they reached 80 to 90 % confluency.

After the primary culture reaching 80-90% confluency, the adherent BM-MSCs cells were detached with a trypsin-EDTA solution (Thermo Fisher Scientific, USA) after being washed twice with PBS, centrifuged at 1500 xg for 5 min, and then reseeded in CCM. Further passages were done until reaching passage 3 (P3). The cells were counted using a hemocytometer under the phase contrast inverted microscope (Olympus CKX41SF, Japan), and their viability was assessed using the trypan blue exclusion test. At P3, the BM-MSCs were employed in this experiment after being trypsin-EDTA solution-detached, suspended in PBS.

Characterization of BM-MSCs

- Inverted phase contrast microscope: was used for daily examination of the cultured cells to assess their morphology and exclude contamination (inverted microscope: Olympus CKX41SF, Japan)[25].

- Colony forming unit fibroblast assay (CFU-F) was done at P3 to characterize BM-MSCs for their proliferation and clonogenic capacity. After fixing the cells, crystal violet stain 3% (Sigma-Aldrich, St. Louis, Missouri, USA) was used to stain them and colonies were seen with a phase contrast inverted microscope[27].

- Immunophenotyping of BM-MSCs by fluorescence-activated cell sorting (FACS) flow cytometry analysis

Fluorescent-labeled monoclonal antibodies were used to characterize the surface markers of passage 3 MSCs. The cells were trypsinized and then rinsed with PBS before being incubated for 30 min, in the dark, with different fluorescent-labeled monoclonal antibodies CD 44 PE, CD 90 FITC and CD 45 (Abcam, Cambridge UK)[26,27].

Isolation of EVs[26]

At CERRMA, the conditioned media of BM-MSCs at P3 was collected after culturing of the cells in serum free media (SFM) and incubated for 24 hours. SFM was formed of DMEM low glucose, 1% L-glutamine and 1% penicillin/streptomycin without FBS. After 24 hours, the conditioned medium was collected and kept at −80 °C, and then CCM was supplied to the adherent cells for another 24 hours to feed the cells and preserve the culture. The next day, the CCM was replaced again with SFM for another 24 hours and then collected and stored. This procedure was repeated every other day for 14 days.

By using a differential centrifugation procedure, the EVs were separated from the conditioned media that had been obtained. First, it was centrifuged at 2000 xg for 20 min to precipitate dead cells and cell debris at CERRMA. Then, at the Institute of Graduate Studies and Research (IGSR), Alexandria University, the supernatant was ultracentrifuged at 100.000 xg for 70 minutes (Beckman Coulter Optima XE-100 Ultracentrifuge, roater 50.2 Ti) to form EVs pellet at 4 °C. Finally, at CERRMA, the pellet was redissolved in 100 µl of sterile PBS in the laminar flow hood to form an EVs suspension.

Characterization of EVs[26,28]

• Transmission electron microscope (TEM) was employed to evaluate the size and shape of EVs. A drop of EVs suspension was loaded to copper grids, removed the excess by filter paper, stained with 1% uranyl acetate, dried at room temperature, then studied under TEM at the Electron Microscopy Unit, Faculty of Science, Alexandria University (JEOL- JSM 1400 Plus, Tokyo, Japan).

• Zeta sizer Nanoparticle analyzer was done to measure the average size at Central Lab, Faculty of Pharmacy, Alexandria University (Malvern, UK).

• The total protein content of EVs suspension was measured using the Lowry method, at Biochemistry Department, Faculty of Medicine, Alexandria University. This procedure was repeated 3 times and an average was taken.

In vivo study and experimental design (Figure 1)

Forty-two adult male albino rats (6–8 weeks old, 150–200 g), were bought and kept in regular housing and laboratory settings in the Animal House of Physiology Department, Faculty of Medicine, Alexandria University. The protocol was permitted by the institutional review board of animal experiments of Faculty of Medicine, Alexandria University. Animals were randomly divided as follow
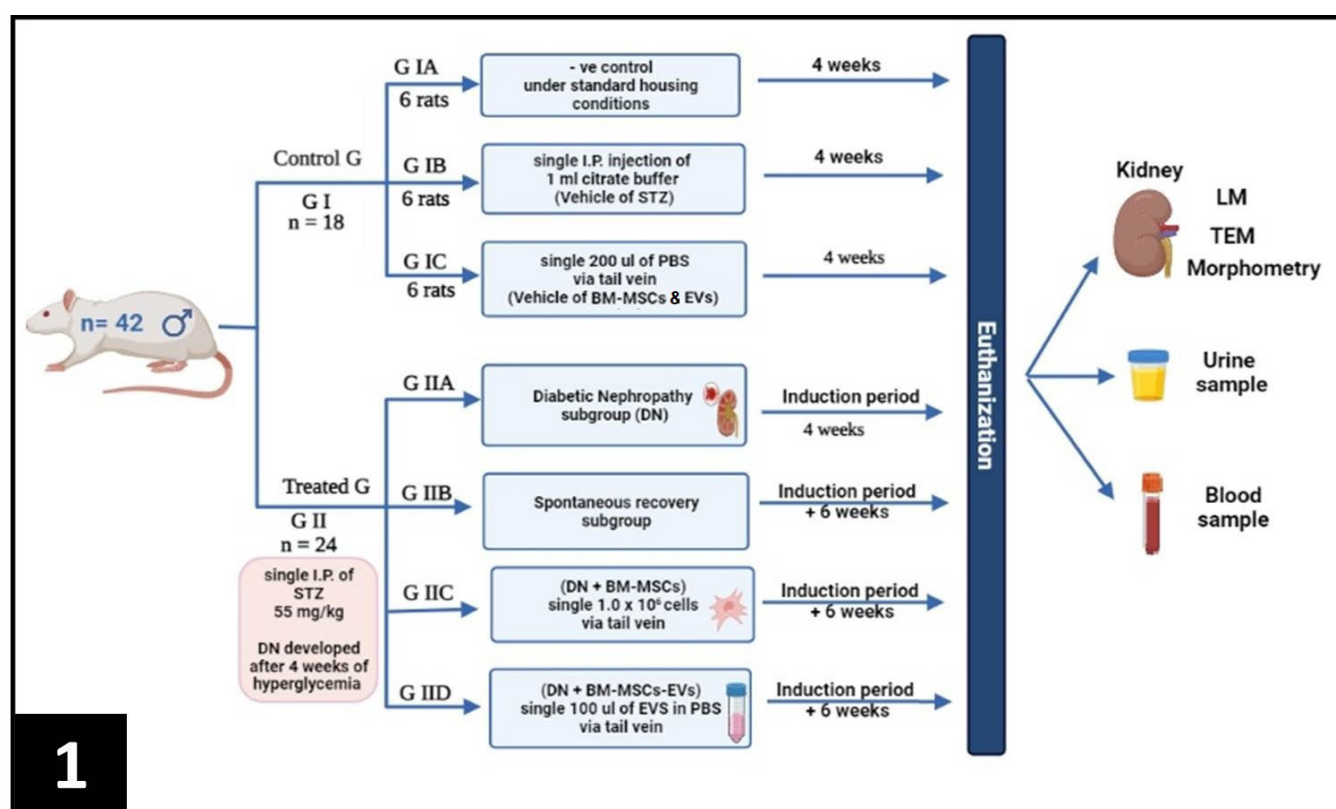

Fig. 1: Diagram representing the in vivo experimental design for the study.

Group I (control group): 18 rats were distributed evenly into 3 subgroups:

- Subgroup IA: 6 rats maintained under standard housing conditions (negative control group).

- Subgroup IB: 6 rats received a single intraperitoneal injection of 1 ml citrate buffer (vehicle of STZ).

- Subgroup IC: 6 rats received a single 200 µl of phosphate buffer saline (PBS) via the tail vein (vehicle of BM-MSCs and EVs).

Animals of the control group were sacrificed by overdose anesthesia (injection of 100 mg/kg phenobarbital) after 4 weeks.

Group II (diabetic group): 24 rats that had been fasting all night got a single dose of streptozotocin (STZ) (55 mg/kg body weight) dissolved in freshly made 0.1 M cold citrate buffer, pH 4.5 by intraperitoneal injection. The following 48 hours after injection, rats were allowed to food and drink with 5% glucose solution to prevent sever hypoglycemia and early death due to massive insulin released from damaged pancreatic β-cells. Blood glucose levels were measured after 3 days of injection. The rats with blood glucose levels less than 250 mg/dl were substituted meanwhile; the diabetic rats with blood glucose > 250 mg/dl were further enrolled in the experiment[29,30] and subdivided evenly into 4 subgroups each of 6 rats:

- Subgroup IIA (DN subgroup): represented the experimental model for diabetic nephropathy. The rats were sacrificed after 4 weeks of injection (induction period).

- Subgroup IIB (spontaneous recovery subgroup): after induction of DN, each rat was left with no further treatment to assess the potential for spontaneous recovery.

- Subgroup IIC (DN + BM-MSCs): following the induction period of DN, each rat received a single dose of 1.0×10^6 BM-MSCs suspended in 1 ml PBS via the tail vein[31,32].

- Subgroup IID (DN + EVs): each rat were given a single dose of 100 µg BM-MSC-EVs dissolved in PBS via the tail vein following the induction period of DN[33].

Animals of subgroups IIB, IIC and IID were sacrificed after anesthesia (100 mg/kg phenobarbital) 6 weeks later.

Biochemical analysis

Assessment of kidney functions

At the end of each experimental period, 24-hour urine was taken before scarification to assess urine protein (mg/dl) using lowry method. Then, the rats were anesthetized using phenobarbital and blood samples were got from the abdominal aorta, centrifuged at 5000 xg for 10 min and the sera were served at measurement of blood urea nitrogen (mg/dl) using enzymatic colorimetric method according

to the manufacturers' manual and serum creatinine (mg/dl) using kinetic reaction method according to the manufacturer's protocol[29,30,34].

Oxidative stress parameters

Serum malondialdehyde (MDA) and total antioxidant capacity (TAC) were assessed from sera samples according to manufacturers' instructions to assess oxidative and antioxidative serum levels using colorimetric method[35].

Inflammatory marker, Interleukin- 6 (IL-6)

According to the manufacturer's instructions (Biosciences, San Diego, USA), ELISA kits were applied to measure the levels of the inflammatory cytokine IL-6 in all animals. Anti-IL-6 polyclonal antibody and biotin conjugated anti-IL-6 polyclonal antibody were employed as detecting antibodies. After the avidin-biotin-peroxidase complex was added, TMB substrate was added. The absorbance was measured at 450nm[36].

Histological methods

Both kidneys were dissected out from each rat carefully and processed for:

Light microscopic study

One kidney from each rat was obtained. 10% neutral buffered formalin was used for fixation of the specimens. Then, they dehydrated in ascending grades of alcohol, cleared in xylol, embedded in soft paraffin then in hard paraffin. Hematoxylin and eosin (H&E) and Masson's trichrome stain were applied to 5 µm thick sections of the paraffin blocks containing kidney tissues. Then they examined using the light microscopy at CERRMA (Olympus Tokyo, Japan, BX41)[37].

Electron microscopic study

From each rat, the other kidney was immediately cut into small cubes of (0.5-1 mm3), fixed in 3% phosphate buffered glutaraldehyde at 4 °C and post-fixed in 1% osmium tetroxide in phosphate buffer for 1-2 hours. Then, the samples were embedded in epon after being dried with graded ethanol. Ultrathin sections (80 nm thick) were cut. Lead citrate and uranyl acetate were used to stain them after they were placed on copper grids. The kidney tissue was examined by the TEM and digital photomicrographs were taken at the Electron Microscopy Unit, Faculty of Science, Alexandria University[38].

Histo-morphometric study

The thickness of the glomerular basement membrane (GBM) using images taken at x10,000 magnification from electron microscopic sections and the area percent of collagen using images taken at x400 magnification from Masson's trichrome stained slides, were measured using the NIH Fiji© Image J software program. For each group, 10 randomly selected points of the two parameters were measured in 10 different non overlapping fields. The measurements for GBM were taken at the epithelial

side of the GBM and excluding the mesangial area of the glomerular capillary loop. All measurements were statistically analyzed[39,40].

Statistical analysis of the results

The statistical program for social sciences (SPSS, version26.0; IBM, Chicago IL, USA) software package was used to assess the biochemical and morphometric results. The mean between the various subgroups was compared using a one-way ANOVA test and pair-wise comparison was done using Post Hoc Test (Tukey). The data presented as the mean ± SD. $P \leq 0.05$ was considered statistically significant[41].

RESULTS

Characterization of the isolated rat BM-MSCs

After 24 hours of the initial seeding (passage 0; P0), cultured cells appeared rounded, non-adherent of variable sizes (Figure 2a). Seventy-two hours of primary culture (P0), the cells started to be adherent to the culture flask and appeared spindle shape with tapering ends or polygonal with multiple small cytoplasmic processes. Other cells were rounded in shape and floating (Figure 2b). Until passage 3 reached 80–90 % confluency, the cellular shape and proliferative potential were maintained (Figure 2c). The CFU-F assay revealed that the cultivated BM-MSCs have strong clonogenic and proliferative abilities, as evidenced by their accumulation into distinct islands (colonies) that were recognized using crystal violet staining (Figure 2d). The flow cytometric analysis of cell-surface markers of BM-MSCs at P3, showed that 92.02% of cells were positive for anti CD44 and 96.11% of cells were positive for anti CD90, while only 0.17% of cells were positive for anti CD45 (Figures 3a,b)

Characterization of BM-MSCs-EVs

Examination of BM-MSCs-EVs using TEM revealed rounded vesicles of variable sizes surrounded by a lipid bilayer (Figure 4a). The isolated vesicles had a mean size of 221.1 nm and an intensity of 96.8% as measured by Zeta sizer (Figure 4b). The total protein content of the EVs suspension was estimated 473 µg/ml of protein, confirming the efficiency of the isolation protocol and high content of EVs.

Biochemical results

Kidney functions

Regarding the mean levels of blood urea nitrogen (BUN), serum creatinine and urine protein, the various control subgroups (IA, IB and IC) did not show any significant difference statistically. Induction of diabetes in subgroup IIA (DN) led to statistically significant increase in the levels of BUN, serum creatinine and urine protein compared to the control subgroup IA. This increase persisted in subgroup IIB (spontaneous recovery subgroup) with a statistically significant increase compared to subgroup IIA.

On the other hand, the mean levels of BUN, serum creatinine and urine protein revealed a significant decrease in subgroups IIC and IID (DN + BM-MSCs and DN + EVs subgroups respectively), in comparison with subgroups IIA and IIB. While subgroup IIC (BM-MSCs) displayed significant increase in the measured parameters of kidney functions compared to the control subgroups, subgroup IID (DN + EVs) did not show significant difference when compared to the control subgroups. In addition, subgroup IID showed significant improvement of kidney function parameters when compared to subgroup IIC (Histogram 1).

Oxidative stress parameters

a- Serum Malondialdehyde (MDA)

MDA levels in the serum were found to be significantly higher in subgroups IIA and IIB (diabetic nephropathy and spontaneous recovery subgroups respectively) as compared to the control subgroups which showed no statistical difference among them. In addition, subgroup IIB revealed significant increase when compared to subgroup IIA.

Inversely, MDA levels were significantly decreased in subgroups IIC and IID (DN + BM-MSCs and DN + EVs subgroups respectively), in comparison with subgroups IIA and IIB. No significant difference was detected when comparing subgroup IID to the control subgroups with statistically significant decrease when compared to subgroup IIC. (Histogram 2 a)

b- Serum total antioxidant capacity (TAC)

The mean amounts of TAC in the serum were significantly lower in subgroups IIA and IIB (diabetic nephropathy and spontaneous recovery subgroups respectively) as compared to the control subgroup IA. While, the mean level of TAC in subgroup IIB showed significant reduction in comparison to subgroup IIA.

The rats received MSC and EVs (subgroups IIC and IID) exhibited significant rise in the mean TAC levels as compared to DN and spontaneous recovery subgroups (subgroups IIA and IIB). However, rats received EVs (subgroup IID) did not exhibit significant differences compared to the control subgroups with statistically significant increase as compared to rats received MSCs (subgroup IIC). (Histogram 2 b)

c- Serum IL-6

In the present work, the mean serum IL-6 levels did not differ significantly among the control subgroups (IA, IB and IC).

The mean levels of serum IL-6 revealed a significant rise in subgroups IIA, IIB and IIC when compared to the control subgroups. Interestingly, subgroup IIB showed a significant elevation when compared to subgroup IIA, while subgroup IIC revealed a significant decrease in comparison with subgroups IIA.

As regard subgroup IID, there was no significant difference in comparison with control subgroups, while

it showed significant decrease when compared with subgroups IIA, IIB and IIC. (Histogram 2 c)

Light microscopic results (H&E stain)

Group I (control group): In the renal cortex, light microscopic examination of renal corpuscles of control subgroups rats (IA, IB and IC), revealed almost the same normal histological findings. The renal corpuscles contained tufts of glomerular capillaries surrounded by Bowman's capsule. The Bowman's capsule showed an inner visceral layer adherent to the glomerular capillaries and outer parietal layer with Bowman's space appearing between the two layers. The parietal layer appeared as an intact regular outer coat of Bowman's capsule and is made up of simple squamous epithelium with flattened nuclei (Figure 5).

Group II:

1. Subgroup IIA (DN; diabetic nephropathy subgroup): Distorted architecture of renal corpuscles was depicted on light microscopic examination of subgroup IIA. Some renal corpuscles showed hypercellular broadening glomeruli with congested glomerular capillaries, obliteration of Bowman's space and tuft adhesion between parietal cells and podocytes. Others exhibited shrunken glomeruli with widening of Bowman's space. Parietal layer of Bowman's capsule was interrupted while some parietal cells were swollen, enlarged and protruded into Bowman's space. Mesangial matrix expansion appeared as acellular eosinophilic material. Arteriolar hyalinization with thickened wall and periglomerular mononuclear cellular infiltration were also seen (Figures 6 a-d).

2. Subgroup IIB (spontaneous recovery subgroup): Light microscopic analysis of the renal cortex of subgroup IIB showed marked affection of the renal corpuscles' architectures. Shrunken, lobulated glomeruli with marked broadening of Bowman's spaces were noticed. Congested glomerular capillaries were seen. Some parietal cells of Bowman's capsule appeared enlarged and protruded into the Bowman's space. Areas of interrupted parietal layer of Bowman's capsule were also noticed (Figure 7).

3. Subgroup IIC (DN + BM-MSCs): Light microscopic examination of the renal corpuscles of subgroup IIC demonstrated partial restoration of corpuscles architecture. Normal glomerular capillary tufts surrounded by regular intact parietal cell layer were seen. Few foci of mesangial expansion with some congested glomerular capillaries and congested peritubular blood vessel were also observed (Figure 8a).

4. Subgroup IID (DN + BM-MSCs-EVs): When compared to diabetic rats, the renal corpuscles of subgroup IID rats revealed noticeable structural improvement almost regaining the normal histological architecture. The renal corpuscle appeared with regular outline and intact parietal layer of Bowman's capsule. Bowman's space was normal and uniform. Some congested glomerular capillaries were noticed (Figure 8b).

Masson's trichrome stain

Masson's trichrome stained sections of the control subgroups (IA, IB and IC) revealed few collagen fibers mostly around the Bowman's capsule, among the glomerular capillaries and within the narrow peritubular interstitial tissues (Figure 9a).

Subgroup IIA (diabetic nephropathy subgroup) showed a noticeably augmented deposition of the collagen fibers between the glomerular tuft of capillaries. A considerable amount of collagen fibers was observed around the renal corpuscles and in between the renal tubules (Figure 9b). Furthermore, subgroup IIB (spontaneous recovery subgroup) revealed destructive collagen deposition in the intraglomerular tissue between the tuft of capillaries, in Bowman's capsule and around renal tubules (Figure 9c).

Nevertheless, collagen deposition was significantly decreased after injection of BM-MSCs and EVs in subgroup IIC and IID (DN + BM-MSCs and DN + EVs subgroups respectively) with some collagen fiber being seen among the glomerular capillaries in subgroup IIC (Figures 9d, e).

Quantitative morphometric analysis of the area percentage (%) of collagen deposition

Our findings were statistically supported by the results of the morphometric analysis of the area percentage of collagen deposition. Between the various control subgroups (IA, IB and IC), the mean area % of collagen did not show any significant difference ($P<0.05$). Subgroup IIA (diabetic nephropathy subgroup) and subgroup IIB (spontaneous recovery subgroup) rats had a statistically significant increase in the area percent of collagen deposition as compared to the control group with a statistically significant increase in subgroup IIB compared to subgroup IIA. Inversely, on comparing subgroups IIC and IID (DN + BM-MSCs and DN + EVs subgroups respectively) to subgroup IIB, they displayed a significant reduction in the area % of collagen deposition with a statistically significant decrease in subgroup IID compared to subgroup IIC. Meanwhile, subgroup IID did not reveal any significant difference with respect to the control subgroups (Figure 9 f).

Electron microscopic results

Group I (control group): Electron microscopic inspection of ultrathin sections of renal corpuscles of control group revealed normal ultra-structural findings, which were almost the same in all control subgroups (IA, IB and IC). The renal corpuscles were surrounded by an intact parietal layer of attenuated cells with flattened euchromatic nucleus. The renal corpuscles revealed glomerular capillaries lined by fenestrated endothelial cells with attenuated euchromatic nucleus. Podocytes wrapping the glomerular capillaries appeared as large stellate cells with multiple primary cytoplasmic processes. They exhibited euchromatic nucleus, cisternae of rER and multiple mitochondria. Secondary processes

arising from the primary processes of podocytes were numerous, regularly spaced by filtration slits that were bridged with slit diaphragm and resting on the glomerular basement membrane. The glomerular basement membrane appeared thin, regular with a trilamellar pattern; central lamina densa that lies between laminae rara externa and interna. Its thickness was ranging from 98.83- 149.74 nm (Figures 10 a-c).

Group II:

1. Subgroup IIA (diabetic nephropathy subgroup): Ultrastructure examination of renal corpuscles of subgroup IIA demonstrated variable pathological changes. The parietal cells of Bowman's capsule appeared enlarged, protruding into Bowman's space exhibiting vacuolated cytoplasm with focal adhesions to podocytes. The glomerular capillaries appeared congested and surrounded by an irregularly thickened basement membrane. The thickness of GBM was ranging from 275.69 to 990.73 nm. Some lining endothelial cells exhibited dark rounded nucleus that protruded into the capillary lumen. Others showed focal loss of fenestrations. Detached apoptotic endothelial cells from glomerular basement membrane with dark nucleus were also seen. Secondary processes of podocytes appeared irregularly spaced with areas of flattening and effacement, while primary processes showed electron dense deposits. Mesangial cell proliferation was noticed in between the glomerular capillaries. Extensive mesangial matrix deposition appeared between the glomerular capillaries encroaching on their lumina and forming subendothelial deposits. Furthermore, numerous inflammatory cells were seen in the capillary lumina. Some of them exhibited adhesion to the endothelial cells; others showed transmigration with podosome formation (Figures 11 a-f).

2. Subgroup IIB (spontaneous recovery subgroup): Electron microscopic examination of the renal corpuscles of subgroup IIB showed marked ultrastructure affection. The parietal cells of Bowman's capsule appeared enlarged with irregular nuclei, dilated perinuclear cisternae and some cytoplasmic vacuoles. The glomerular capillaries were surrounded by an irregular glomerular basement membrane with focal thickening and loss of the trilamellar pattern. The thickness of GBM was ranging from 401.82 to 1035.17 nm. The lining endothelial cells showed focal loss of fenestration. Moreover, podocytes exhibited multiple mitochondria, dilated cisternae of rER and dilated cisternae of Golgi complex. Most of their secondary processes were irregularly spaced with areas of flattening, effacement and electron dense deposits. Mesangial cells with mesangial matrix expansion were seen encroaching on the capillary lumina. Finally, some inflammatory cells were also noticed inside the capillary lumen (Figures 12 a-d).

3. Subgroup IIC (BM-MSCs treated subgroup): On examining the renal corpuscles of subgroup IIC rats, partial improvement of corpuscles architecture was detected. The parietal cells of Bowman's capsule appeared attenuated with flattened nuclei and some cytoplasmic vacuoles. The glomerular capillaries were surrounded by a nearly thin glomerular basement membrane that exhibited a trilamellar pattern. Focal thickening of GBM was also noticed. The thickness of GBM was ranging from 125.76 to 336.75 nm. The glomerular capillaries were lined by fenestrated attenuated endothelial cells. Podocytes exhibited euchromatic nucleus and multiple of rER. Their primary processes showed multiple lysosomes with myelin figure and electron dense deposits, while their secondary processes appeared numerous regularly spaced, separated by filtration slits and resting on thin glomerular basement membrane. Few secondary processes fused together with flattening. Mesangial cells with irregular euchromatic nuclei were seen in between glomerular capillaries and embedded in the mesangial matrix (Figures 13 a-d).

4. Subgroup IID (BM-MSCs-EVs treated subgroup): Electron microscopic examination of the renal corpuscles of subgroup IID rats exhibited evidently a preserved normal histological ultrastructure of the renal corpuscles. The renal corpuscles were surrounded by attenuated parietal cells with flattened euchromatic nuclei. The glomerular basement membrane appeared thin and regular with a trilamellar pattern. Focal thickening of GBM was also notice. The thickness of GBM was ranging from 103.70 to 192.34 nm. The glomerular capillaries were lined by fenestrated endothelial cells with attenuated euchromatic nucleus. Podocytes exhibited euchromatic irregular nucleus, multiple cisternae of rER, numerous mitochondria and large autophagolysosome. Most of their secondary processes appeared regularly spaced, while few showed fusion and flattening. Mesangial matrix was noticed between the glomerular capillaries (Figures 14 a- c).

Histo-morphometric results of GBM thickness

The mean levels of glomerular basement membrane thickness in the different control subgroups (IA, IB and IC) were almost the same with no significant difference in subgroup IB and IC as compared with subgroup IA (at $P \leq 0.05$). There was a significant increase in the mean values of GBM thickness in subgroups IIA and IIB when compared to the control subgroups.

In subgroups IIC and IID (the treated subgroups with BM-MSCs and BM-MSCs-EVs respectively), the mean levels of GBM thickness showed a significant decrease comparable to subgroups IIA and IIB. However, there was no significant difference in the values of subgroups IIC and IID in comparison with control subgroups (at $P \leq 0.05$) (Histogram 3)
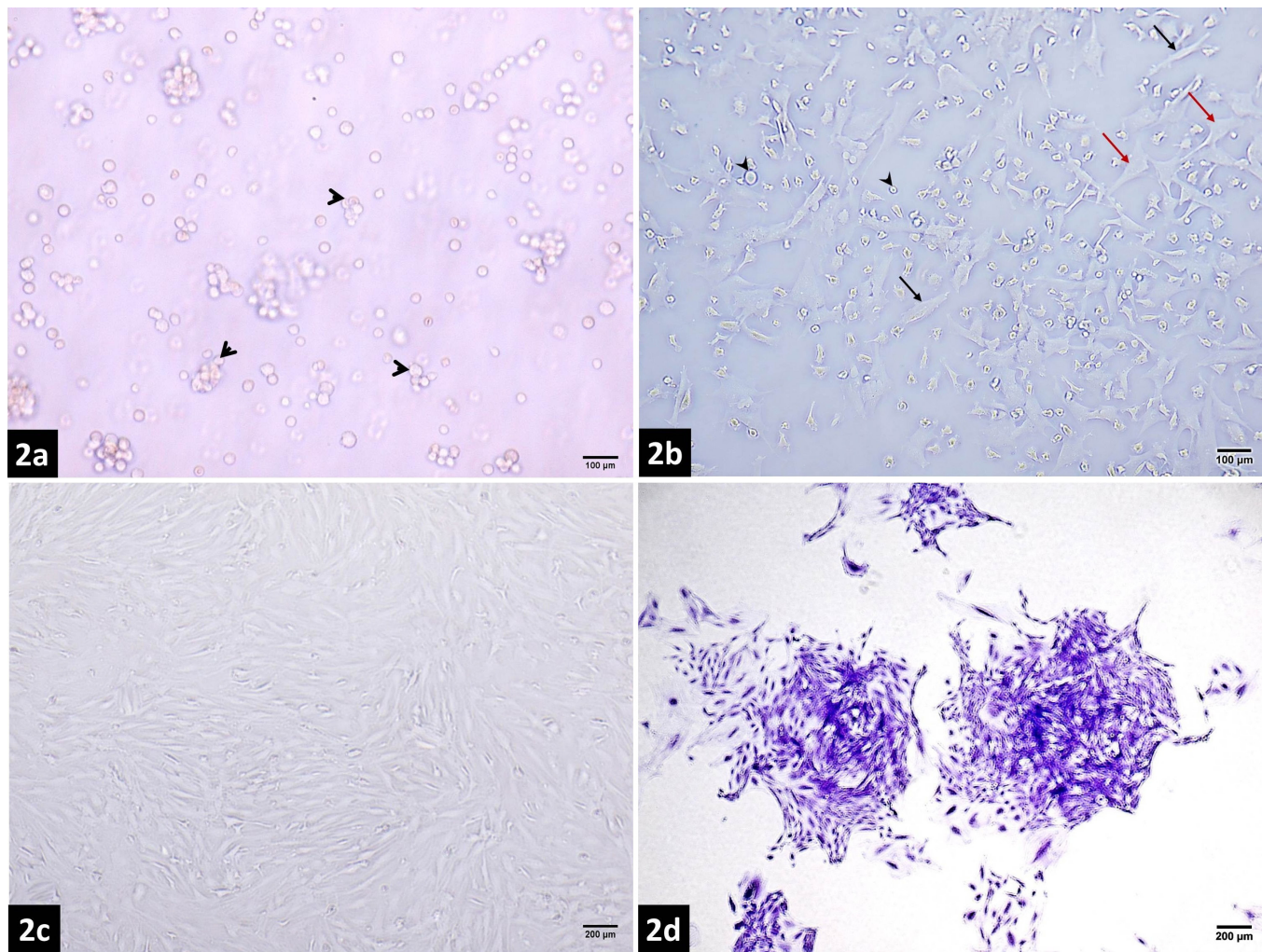
Fig. 2a-d: Representative light photomicrographs characterization of BM-MSCs: a) Passage zero (P0) of BM-MSCs after 24 hours of the initial seeding, showing rounded, non-adherent cultured cells of variable sizes (arrow heads). b) P0 after 72 hours of cultivation, displaying some adherent cells, with either spindle (black arrows) or flat polygonal (red arrows) shapes. Other cells appear small rounded and floating (arrowheads). c) P3 with about 80-90% confluency. d) CFU-F assay for P3 cultured cells, showing colonies formation with crystal violet stain. (Phase contrast inverted microscope, Mic. Mag. a,b: x200, c,d: x100).
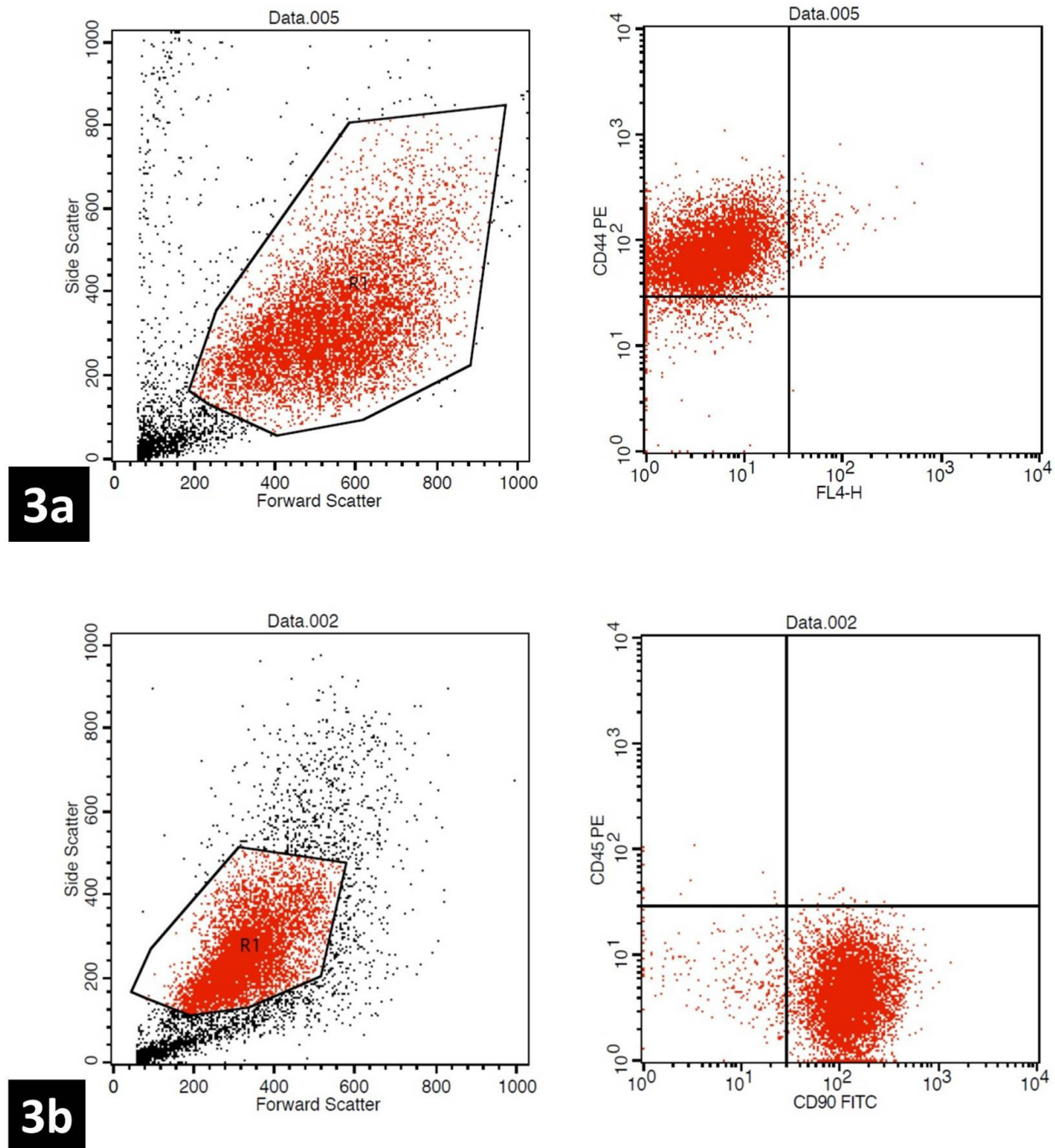
Fig. 3a, b: Scattered plot charts for flow cytometric analysis of cell-surface markers of BM-MSCs at P3. a: 92.02% of the cultivated cells displayed the MSC marker (CD44) (upper left quadrant). b: 96.11% of the cultured cells exhibited the MSC marker (CD90) (lower right quadrant), while only about 0.17% of the cultured cells were positive for the hematopoietic marker (CD45) (upper left quadrant).

4a

155.69nm

156.59nm

126.76nm

150.28nm

100.0nm

1.0μm

**4b**

Size Distribution by Intensity
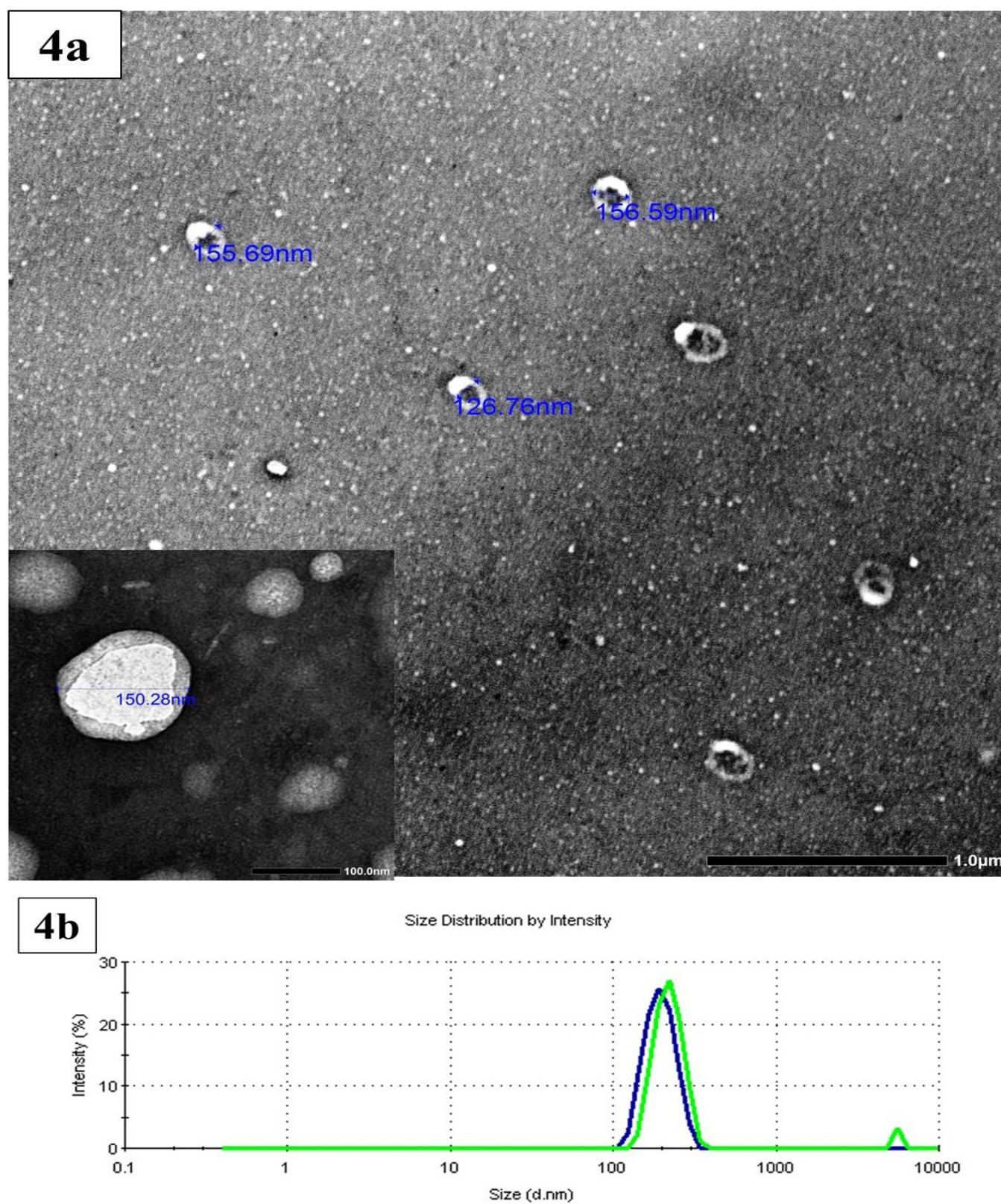
Fig. 4a, b: Characterization of MSCs-EVs. a: A transmission electron photomicrograph of EVs' suspension, showing rounded membranous vesicles of variable sizes. Inset: Higher magnification illustrating a single vesicle surrounded by a lipid bilayer of a 150.28 nm size. (Mic. Mag. a: x12.000, inset: x60.000). b: The size distribution of EVs by Zeta sizer.
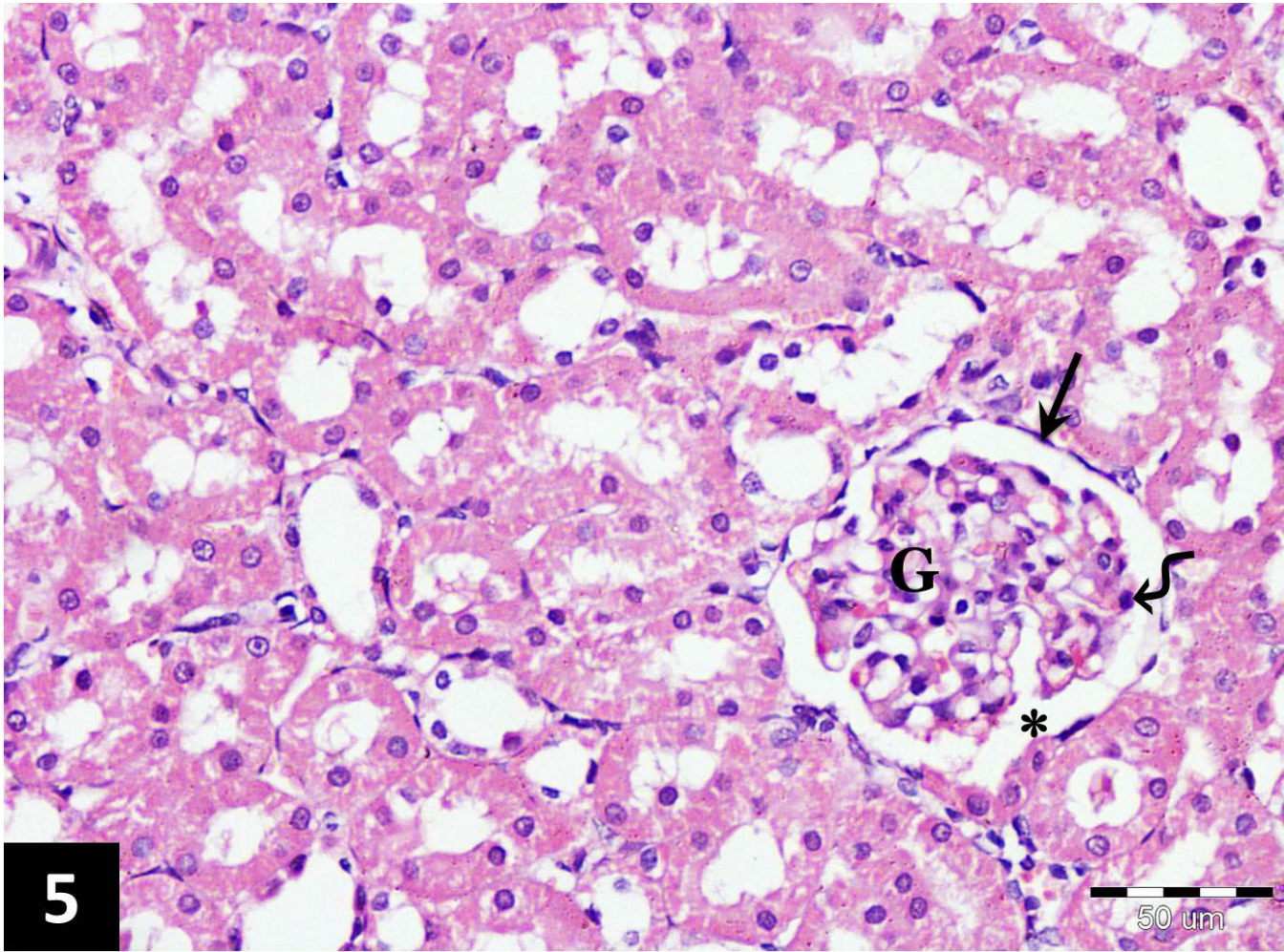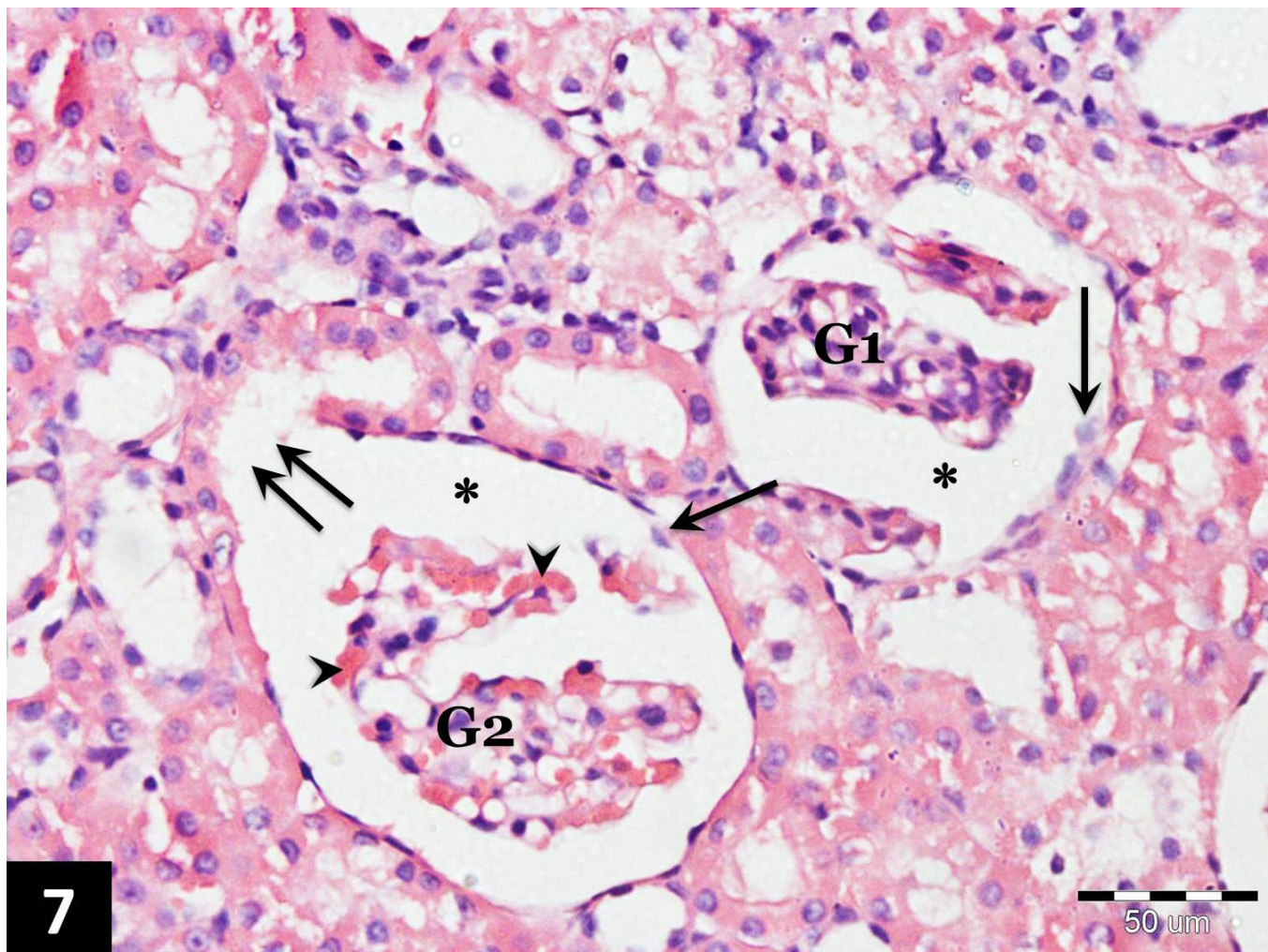
Fig. 5: Light photomicrograph of the renal cortex of the control subgroup IA, revealing a renal corpuscle with a glomerulus (G) containing a tuft of capillaries. The parietal layer of Bowman's capsule is made up of simple squamous epithelium with flattened nuclei (arrow). The visceral layer is adherent to the glomerular capillaries (wavy arrow). ; Bowman's space. H&E stain (Mic. Mag. x400)
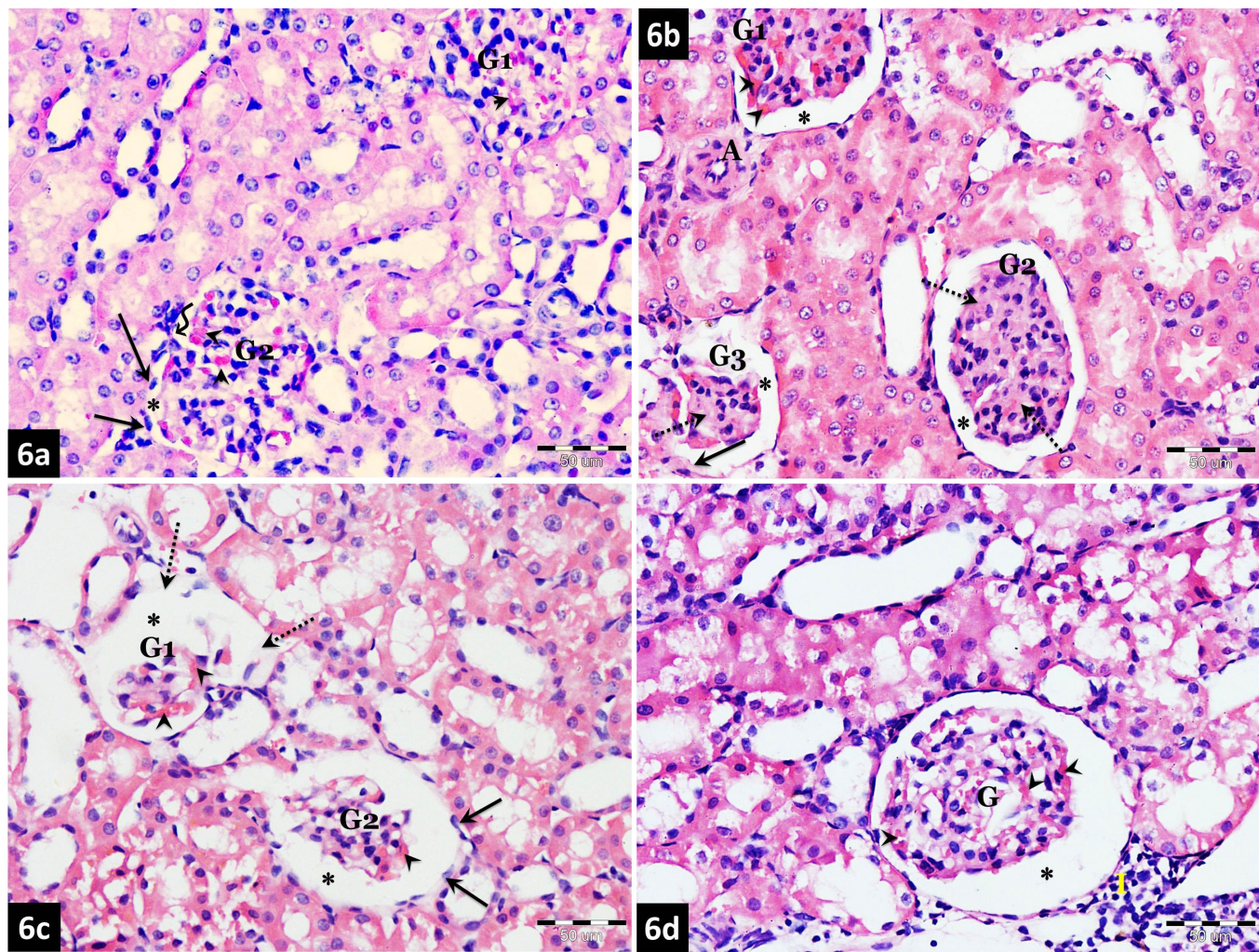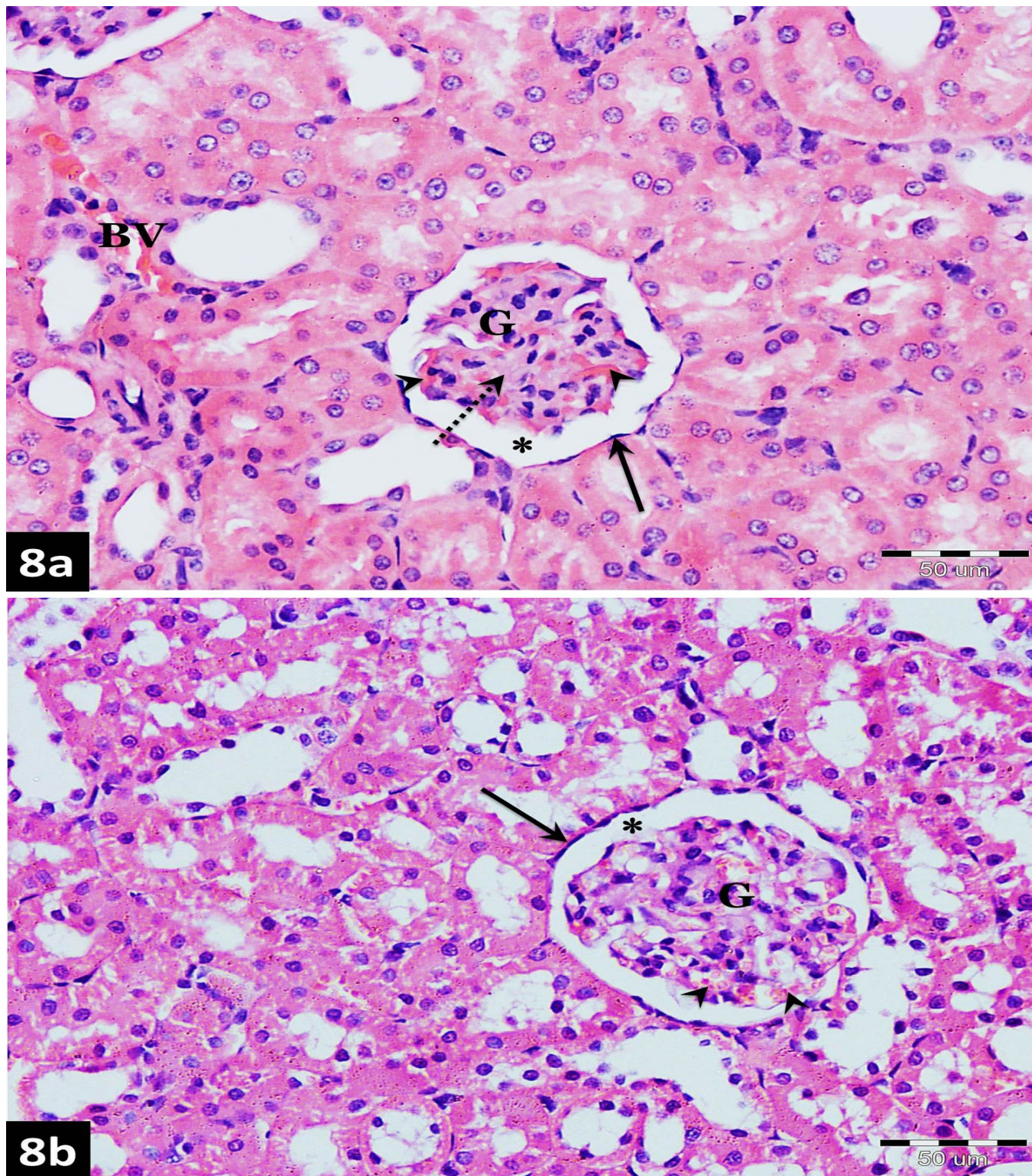
Fig. 6a-d: Light photomicrographs of the renal cortex of subgroup IIA (diabetic nephropathy subgroup) showing: a&b) hypercellular glomeruli (G1 & G2) with congested capillaries (arrowheads). Some parietal cells of Bowman's capsule appear with enlarged nuclei and protruding into the Bowman's space (arrows). Broadening of renal glomeruli with obliteration of Bowman's spaces (*) and tuft adhesion (wavy arrows) in a. Mesangial matrix expansion (dotted arrows) and arteriolar hyalinization with thickening of the wall of arteriole (A) are seen in b. c) distorted renal corpuscles with shrunken glomeruli (G1 & G2) and widening of Bowman's space (^). Interrupted parietal layer of Bowman's capsule (dotted arrows) while other parietal cells are swollen (arrows). (^) congested glomerular capillaries. d) periglomerular mononuclear cellular infiltration (I) and congested glomerular capillaries (arrowheads). Bowman's space (*) shows marked widening. G; glomerulus. H&E stain (Mic. Mag. a-d x400)

Fig. 7: Light photomicrograph of the renal cortex of subgroup IIB (spontaneous recovery subgroup), illustrating renal corpuscles with shrunken lobulated glomeruli (G1 and G2) and congestion of intraglomerular capillaries (arrowheads) in G2. Bowman's spaces show marked widening (*). Some parietal cells appear enlarged and protruding into the Bowman's space (arrows). Note; area of interrupted parietal layer of Bowman's capsule (double arrow). H&E stain (Mic. Mag. x400)

Fig. 8a, b: Light photomicrographs of the renal cortex: a) subgroup IIC (DN + BM-MSCs) showing a regular intact layer of parietal cells of the Bowman's capsule (arrow). Foci of mesangial expansion are also noticed (dotted arrow). Congested intraglomerular capillary tufts (arrowheads) and peritubular blood vessel (BV) are additionally seen. *; Bowman's space. b) Subgroup IID (DN + EVs) showing restoration of normal glomerulus architecture (G) with intact regular parietal layer of Bowman's capsule (arrow). Bowman's space appears normal and regular (^). (^) congested glomerular capillaries. H&E stain (Mic. Mag. a&b x400)
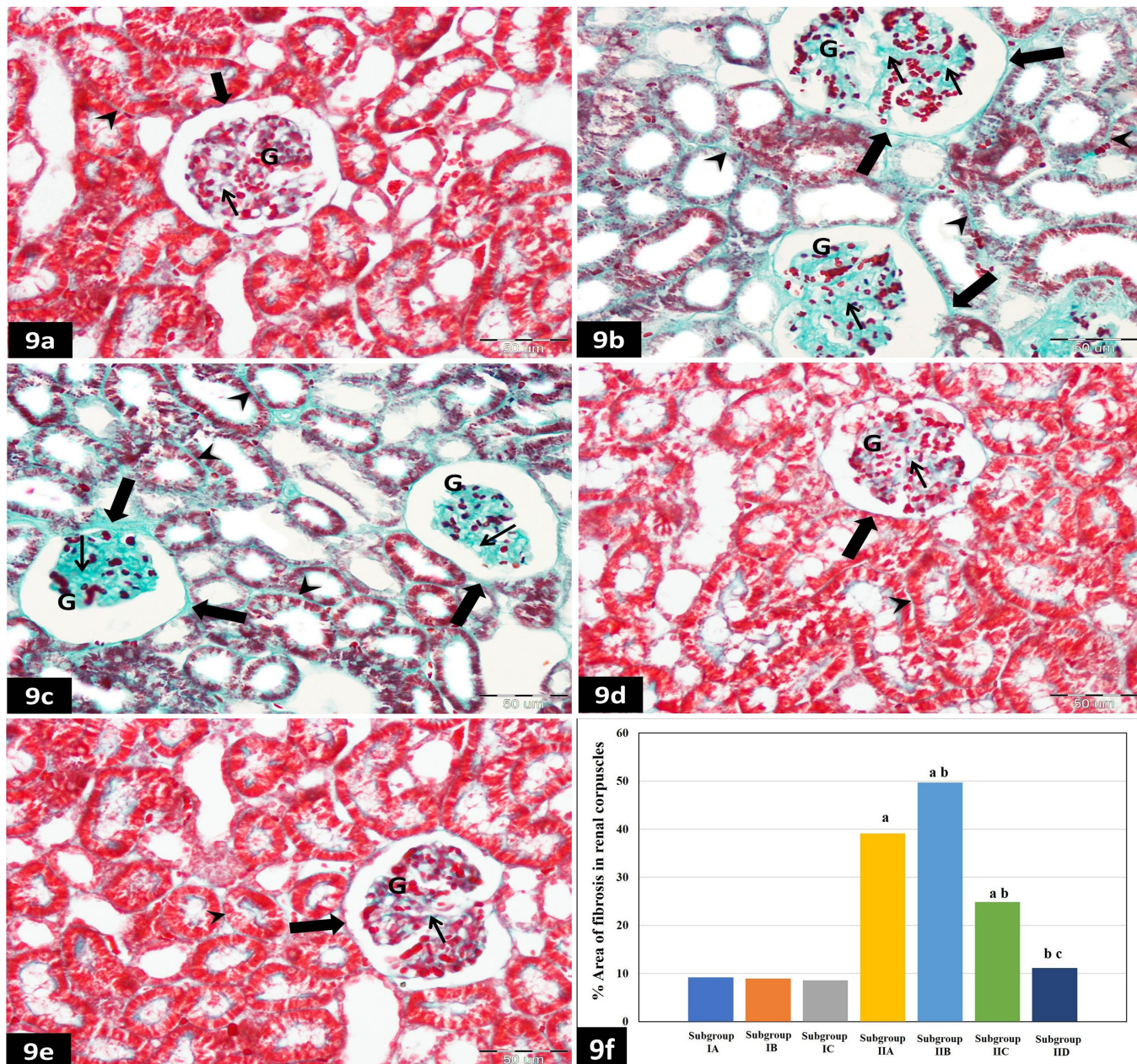
Fig. 9 a-e: Photomicrographs of Masson's trichrome stained renal cortex sections. a) Control subgroup IA: normal distribution of tiny collagen fibers around the Bowman's capsule (thick arrow), between the glomerular tuft of capillaries (thin arrow) and in the interstitium between the renal tubules (arrowhead). b& c) Subgroups IIA and IIB (diabetic nephropathy and spontaneous recovery subgroups) showing extensively expanded deposition of collagen fibers in the intraglomerular tissue between the tuft of capillaries (thin arrows) with evident increase deposition in pericapsular areas around the renal corpuscles (thick arrows) and the interstitium in peritubular areas (arrowheads). d&e) Subgroups IIC and IID (DN + BM-MSCs and DN + EVs respectively): noticeable decrease in collagen fibers is seen around the Bowman's capsule (thick arrow) and in between the renal tubules (arrowhead). Some collagen fiber among the glomerular capillaries (thin arrow) is still seen in d, while normal distribution of collagen deposition nearly similar to the control group in e. G; glomerulus. Mic. Mag. a-e x400

f: A Histogram depicting the morphometric statistical analysis comparison between the subgroups investigated based on the mean area percent of collagen deposition. a; indicates significant statistical difference compared to the control subgroup IA. b; indicates significant statistical difference compared to the diabetic nephropathy subgroup. c; indicates significant statistical difference compared to subgroup IIC ($P \leq 0.05$).
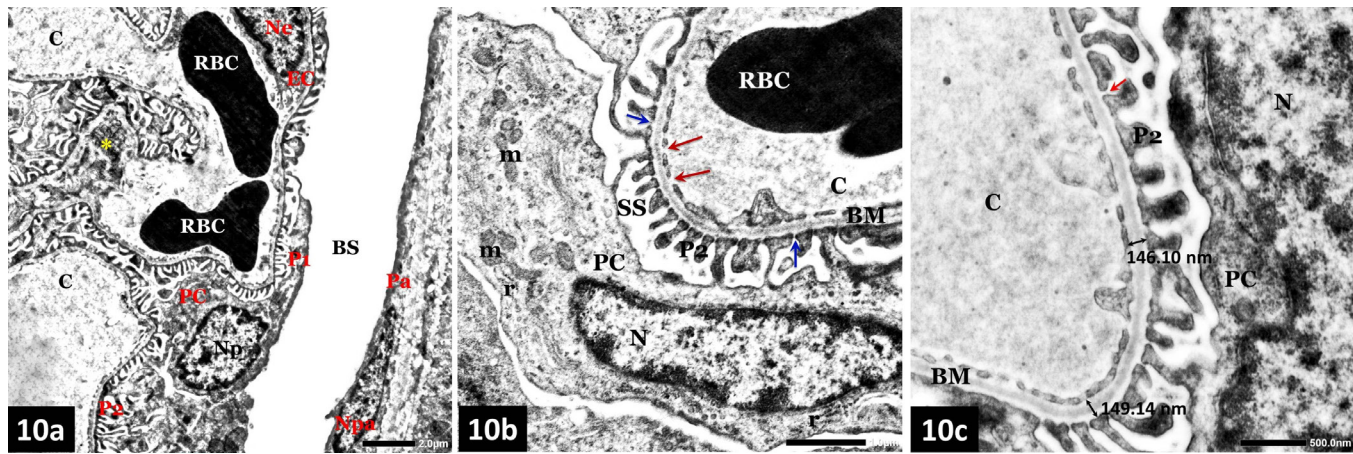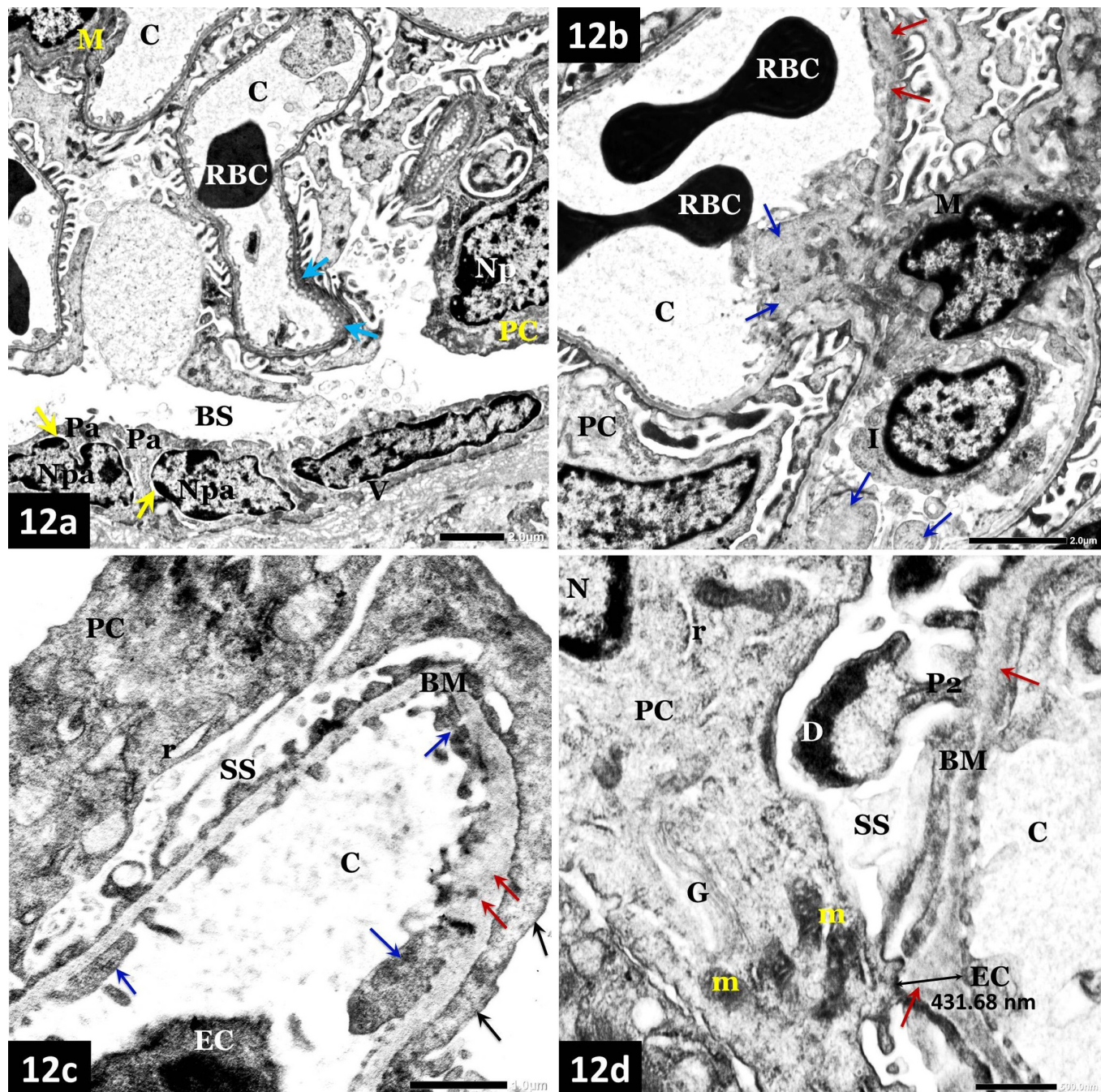
Fig. 10 a-c: Electron micrographs of a renal corpuscle of the control subgroups (subgroups IA, IB and IC) showing: a) Glomerular capillary (C) lined by endothelial cells (EC) with euchromatic nucleus (Ne) and surrounded by a podocyte (PC). The podocyte (PC) exhibits euchromatic nucleus (Np) and numerous regularly spaced secondary processes (P2) arising from primary processes (P1). Parietal cell (Pa) appears attenuated with flattened euchromatic nucleus (Npa). Mesangial matrix (*) is seen between glomerular capillaries. RBC; red blood corpuscle. BS; Bowman's space. b) Glomerular capillary (C) lined by fenestrated (red arrows) endothelial cells and surrounded by a podocyte (PC) is noticed. The podocyte (PC) exhibits multiple mitochondria (m) and cisternae of rER (r). The glomerular basement membrane (BM) appears with a trilamellar pattern; central lamina densa lying between laminae rara externa and interna. Numerous secondary processes (P2) are regularly spaced by filtration slits (blue arrows) and resting on the glomerular basement membrane. RBC; red blood corpuscle. SS; subpodocytic space. N; nucleus of podocyte. c) The glomerular basement membrane (BM) appears regular and thin with thickness about 146.10 nm. Secondary processes (P2) are regularly spaced by filtration slits bridged with slit diaphragm (red arrow) C; capillary. PC; podocyte. N; nucleus of podocyte. Mic. Mag. a) x 2000, b) x 6000, c) x 10.000.
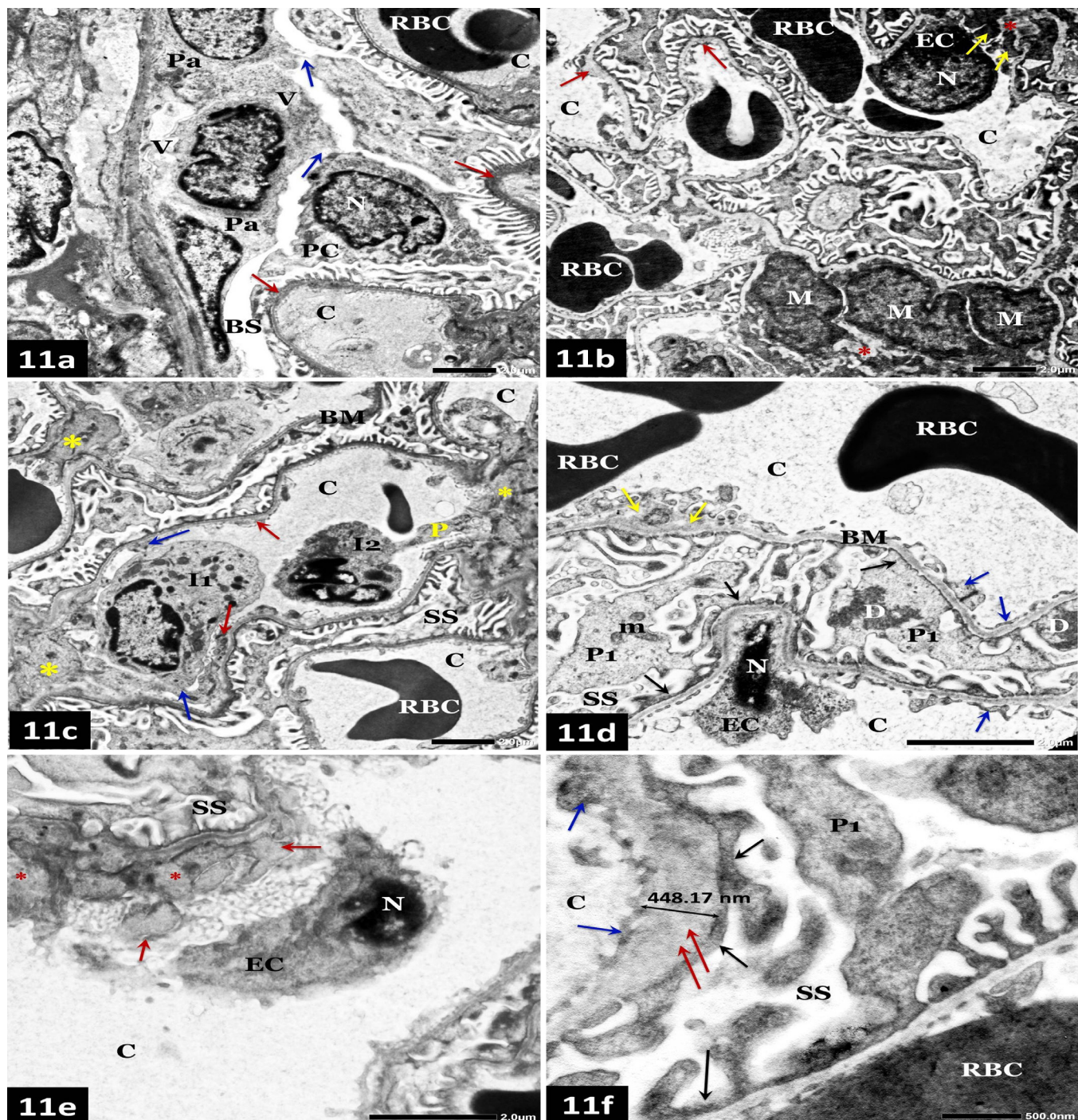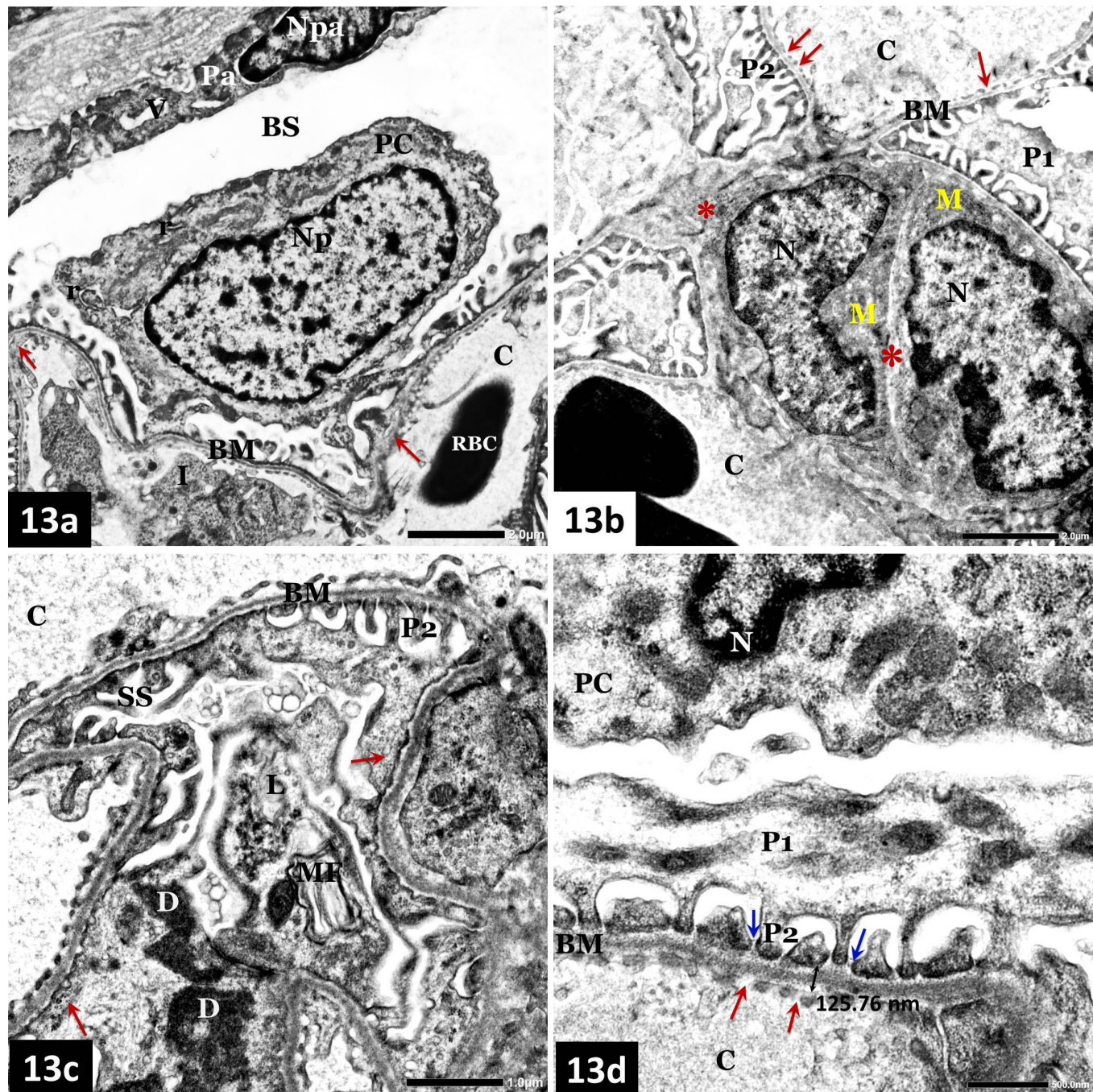
Fig. 11 a-f: Electron micrographs of renal corpuscles of subgroup IIA (diabetic nephropathy subgroup) revealing: a) Parietal cells (Pa) are enlarged and protruding into Bowman's space (BS). They exhibit vacuolated cytoplasm (V) and focal adhesions with podocytes (blue arrows). Podocyte (PC) appears with indented nucleus (N). The glomerular capillaries (C) are surrounded by glomerular basement membrane with focal thickening (red arrows). RBC; red blood corpuscle. b) Mesangial cells proliferation (M) is seen in between glomerular capillaries with mesangial matrix expansion (*) encroaching on the capillary lumina (yellow arrows). The glomerular basement membrane shows focal thickening (red arrows). Endothelial cell (EC) appears with dark rounded nucleus (N) protruding into the capillary lumen (C). RBC; red blood corpuscle. c) Numerous inflammatory cells (I1 & I2) are seen in the capillary lumen adhering to the endothelial cells (blue arrows) with podosome formation (P) in I2. Glomerular capillaries (C) are surrounded by irregular basement membrane (BM) with subendothelial deposits (red arrows). Increased mesangial matrix (*) is also noticed between the glomerular capillaries. RBC; red blood corpuscle. SS; subpodocytic space. d) The lining endothelial cell (EC) of a glomerular capillary (C) appears with dense heterochromatic nucleus (N). Focal areas of non-fenestrated endothelium (blue arrows) with subendothelial deposits (yellow arrows) are seen. Some secondary processes of podocyte are irregularly spaced with areas of flattening and fusion (black arrows). Primary processes of podocyte (P1) show electron dense deposits (D) and mitochondria (m). BM; basement membrane, RBC; red blood corpuscle, SS; subpodocytic space. e) Detached apoptotic endothelial cell (EC) from glomerular basement membrane exhibiting dark nucleus (N). Mesangial matrix (*) encroaching on the glomerular capillary lumen (red arrows) is also seen. SS; subpodocytic space, C; glomerular capillary. f) The glomerular basement membrane exhibits focal thickening (red arrows) about 448.17 nm thick. Secondary processes of podocyte are irregularly spaced with areas of flattening and effacement (black arrows). Focal loss of fenestrations (blue arrows) of endothelial cells is also detected. RBC; red blood corpuscle, P1; Primary process, SS; subpodocytic space. Mic. Mag. a, b& c) x 2000, d&e) x 4000, f) x 10.000
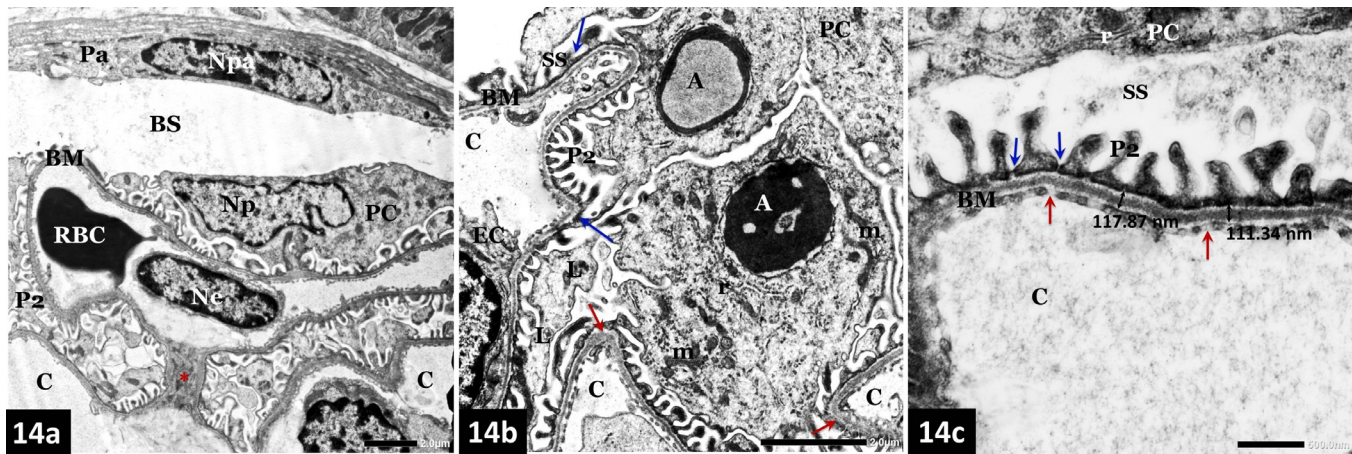
Fig. 12 a-d: Electron micrographs of renal corpuscles of subgroup IIB rats (spontaneous recovery subgroup) illustrating: a) Glomerular capillaries (C) surrounded by irregular glomerular basement membrane with focal thickening (blue arrows). Parietal cells (Pa) appear enlarged with irregular nuclei (Npa), dilated perinuclear cisternae (yellow arrows) and cytoplasmic vacuoles (V). M; mesangial cell, PC; podocyte, Np; nucleus of podocyte, RBC; red blood corpuscle, BS; Bowman's space. b) Mesangial cell (M) and matrix expansion are encroaching on the capillary lumina (blue arrows). Inflammatory cell (I) is noticed inside the capillary (C). Focal thickening of the glomerular basement membrane (red arrows) is also seen. PC; podocyte, RBC; red blood corpuscle. c) Glomerular basement membrane with loss of the trilamellar structure (BM) and focal thickening (red arrows). Podocyte (PC) appears with dilated cisterna of rER (r). Secondary processes of podocyte are seen fused together with flattening and effacement (black arrows). Focal loss of fenestration (blue arrows) of the endothelial cells is also noticed. SS; subpodocytic space, EC; endothelial cell. d) Podocyte (PC) with multiple mitochondria (m), dilated cisternae of rER (r) and dilated cisternae of Golgi complex (G). Electron dense deposits are seen (D) in podocyte's processes. The glomerular basement membrane (BM) shows focal thickening (red arrows) about 431.68 nm thick. SS; subpodocytic space, N; nucleus of podocyte. Mic. Mag. a) x 2000, b) x 3000, c) x 6000, d) x 10.000.

Fig. 13 a-d: Electron micrographs of renal corpuscles of subgroup IIC rats (DN + BM-MSCs subgroup) illustrating: a) A glomerular capillary (C) surrounded by nearly thin glomerular basement membrane (BM) with focal thickening (red arrows). Podocyte (PC) exhibits euchromatic nucleus (Np) and multiple of rER (r). Parietal cell (Pa) is attenuated with flattened nucleus (Npa) and cytoplasmic vacuoles (V). RBC; red blood corpuscle. I; inflammatory cell, BS; Bowman's space. b) Mesangial cells (M) with irregular euchromatic nuclei (N) embedded in mesangial matrix (*). Glomerular capillaries (C) lined by fenestrated endothelial cells (red arrows) are also seen. BM; basement membrane, P1; primary process of podocyte, P2; secondary processes. c) Multiple lysosomes (L), myelin figure (MF) and electron dense deposits (D) are seen in podocyte's processes. The glomerular basement membrane (BM) retains its trilamellar pattern. Some secondary processes (P2) of podocyte appear regularly spaced while others appear with flattening and effacement (red arrows). SS; subpodocytic space, C; glomerular capillary. d) Regular thin glomerular basement membrane (BM) about 125.76 nm thick with a trilamellar structure. A glomerular capillary (C) lined by fenestrated (red arrows) endothelial cells is also seen. Numerous regularly spaced secondary processes (P2) are resting on the glomerular basement membrane and separated by filtration slits (blue arrows). PC; podocyte, N; nucleus of podocyte, P1; primary process of podocyte. Mic. Mag. a&b) x 3.000, c) x 6000, d)x 10.000.

Fig. 14 a-c: Electron micrographs of renal corpuscles of subgroup IID rats (BM-MSCs-EVs subgroup) revealing: a) Glomerular capillaries (C) lined by fenestrated endothelial cells with euchromatic nucleus (Ne). Podocyte (PC) exhibits euchromatic irregular nucleus (Np). Attenuated parietal cell (Pa) with flattened euchromatic nucleus (Npa) is also seen. Mesangial matrix is noticed (*) between the glomerular capillaries. BM; basement membrane, P2; secondary processes, RBC; red blood corpuscle, BS; Bowman's space. b) A podocyte (PC) surrounding glomerular capillaries (C) is seen with large autophagolysosomes (A), cisternae of rER (r), numerous mitochondria (m) and multiple lysosomes (L). Restoration of numerous regularly spaced secondary processes (P2) with focal area of flattening (blue arrows) is also seen. The glomerular capillaries are surrounded by nearly normal glomerular basement membrane (BM) with a trilamellar pattern. Focal thickening of glomerular basement membrane (red arrows) is also noticed. SS; subpodocytic space, EC; endothelial cell. c) Restoration of nearly regular thin glomerular basement membrane (BM) about 117.87 nm thick. Notice a glomerular capillary (C) lined by fenestrated (red arrows) endothelial cells and surrounded by regularly spaced secondary processes (P2) of podocyte (PC). r; rER, SS; subpodocytic space, Blue arrows; filtration slit. Mic. Mag. a) x2000, b)x4000, c)x 10.000
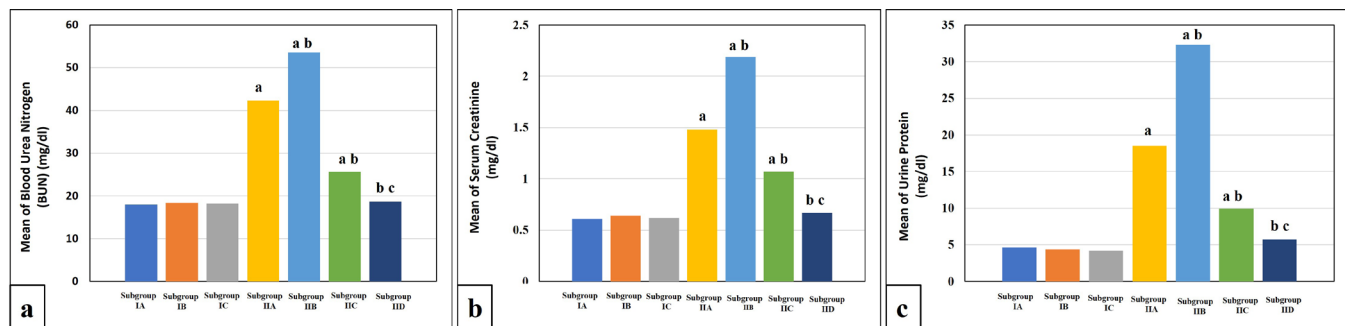
Histogram 1: The mean values of a; blood urea nitrogen (BUN), b; serum creatinine and c; urine protein among the studied subgroups. a; indicates significant statistical difference compared to the control subgroup IA. b; indicates significant statistical difference compared to the diabetic nephropathy subgroup. c; indicates significant statistical difference compared to subgroup IIC (*P*≤0.05).
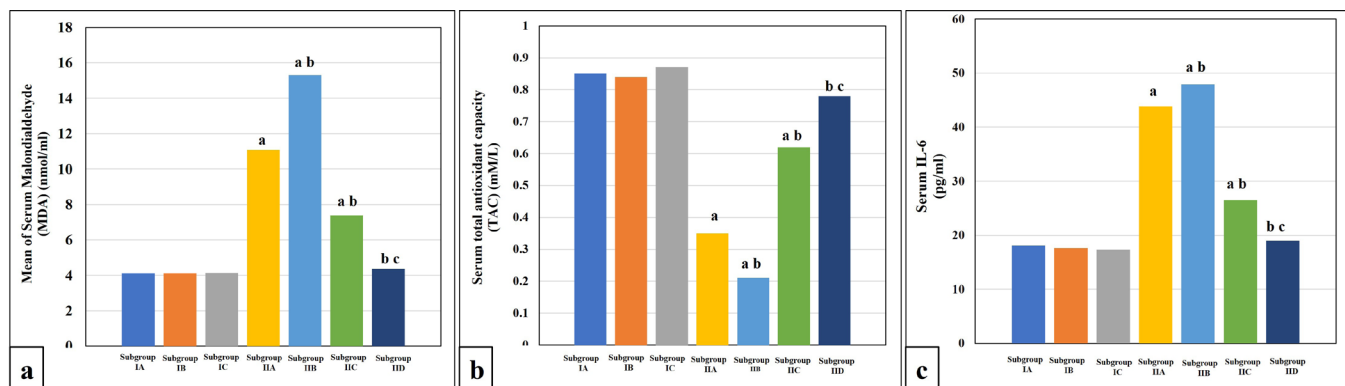
Histogram 2: The mean values of serum a; malondialdehyde (MDA), b; total antioxidant capacity (TAC) and c; IL-6 among the experimental subgroups. a; indicates significant statistical difference compared to the control subgroup IA. b; indicates significant statistical difference compared to the diabetic nephropathy subgroup. c; indicates significant statistical difference compared to subgroup IIC (*P*≤0.05).
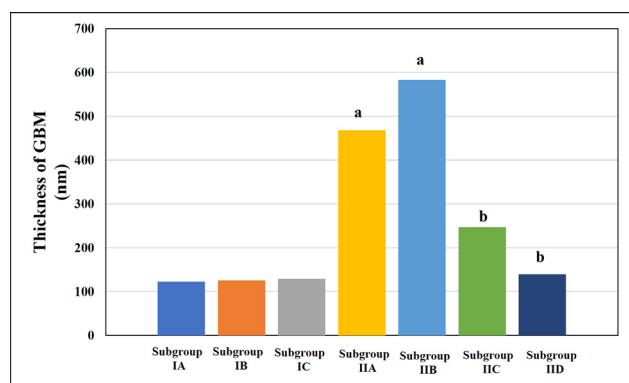
Histogram 3: Comparison of the examined subgroups based on the mean glomerular basement membrane thickness (GBM). a; indicates significant statistical difference compared to the control subgroup IA. b; indicates significant statistical difference compared to the diabetic nephropathy subgroup ($P \leq 0.05$).

DISCUSSION

Diabetes is one of the common syndromes whose commonness is increasing massively worldwide. Diabetic nephropathy (DN) is a chronic, progressive frustrating catastrophe of DM which is a multifactorial disorder characterized by various metabolic and hemodynamic imbalances[42]. In many populations, it is regarded as the most frequent cause of end-stage kidney disease (ESKD), accounting for 28% of people starting renal replacement therapy (RRT) in the United Kingdom, and 44% in the United States and 38% in Australia[43,44].

In the current work, diabetes was induced by intraperitoneal injection of streptozotocin (STZ) in rats. STZ-induced pancreatic damage is regarded a classic animal model for diabetes mellitus type I. Its gains were mostly similar to those observed in human diabetic nephropathy[45]. STZ induces selective cytotoxicity to pancreatic β cells via binding to glucose transport protein 2 (GLUT2) on their cell membrane, thus eliciting structural damage of β-cells, alkylation and methylation of its DNA and cellular oxidative stress with subsequent hyperglycemia[46,47].

Conventional current therapies are not totally competent in the medication of DN, suggesting that auxiliary understanding of the molecular basis of the pathogenesis of DN is vital for the value-added therapy of this disease.

In the current research, light and electron microscopic examination of diabetic nephropathy subgroup (subgroup IIA) revealed hypercellular glomeruli with mesangial cell proliferation and mesangial matrix expansion encroaching on the glomerular capillaries' lumina and forming subendothelial deposits in many renal corpuscles. Also, the glomerular basement membrane appeared irregularly thickened with loss of the trilamellar pattern. This was confirmed by morphometric analysis.

According to Nasef and M Khateib[34] diabetic nephropathy is caused by an interplay between advanced glycation end products (AGEs) and oxidative stress (OS).

Chronic hyperglycemia induces formation of AGEs via non-enzymatic binding of sugars to amino acid groups of proteins, nucleic acids and lipoproteins[48]. AGEs bind to receptors on macrophage cells, podocytes, and tubular cells resulting in a release of a huge portion of reactive oxygen species (ROS), which damages cells by upsetting the equilibrium between the antioxidant and oxidative systems[49].

Moreover, AGEs enhance transcription of several factors as transforming growth factor β1 (TGF-β1), insulin-like growth factor I, II (IGF) and platelets derived growth factor (PDGF). These factors stimulate synthesis of several extracellular matrix components as collagen I, IV, laminin and fibronectin causing mesangial expansion, glomerulosclerosis, GBM thickening as well as subendothelial deposits[50] which were confirmed by Masson's trichrome stain in the present research. Furthermore, AGEs can enhance the expression of the angiotensin II (Ang II) receptors[51]. Angiotensin II enhances protein permeability in glomerular capillaries and stimulates mesangial cell proliferation and mesangial matrix buildup[52].

In addition, persistent hyperglycemia stimulates collateral pathways for glucose metabolism such as the polyol, hexosamine and protein kinase C (PKC) pathways. Stimulated polyol pathway induces increase of ROS production and cellular damage[53]. Also, activated hexosamine and PKC pathways stimulate mesangial cell for expression of several molecules such as TGF-β, fibronectin, endothelin-1 and vascular endothelial growth factor (VEGF) resulting in mesangial matrix expansion and GBM thickening[54].

Another important postulated mechanism of diabetic nephropathy is that chronic hyperglycemia induces inhibition of pro-autophagic transcription factor EB (TFEB) with subsequently suppression of autophagy pathway, accumulation of extracellular matrix and disruption of the GBM integrity[55,56].

In the present study, light microscopic examination of renal corpuscles of subgroup IIA revealed congested glomerular capillaries with periglomerular mononuclear cellular infiltration. This finding was confirmed ultrastructurally by presence of numerous inflammatory cells inside capillary lumina with adhesion to endothelial cells and transmigration with podosome formation. The inflammatory process is an important postulated mechanism of diabetic kidney injury. The accumulated AGEs and ROS activate nuclear factor κB (NF-κB) that enhance transcription of inflammatory gene such as IL-6, TNF-α and monocyte chemoattractant protein-1 (MCP-1) with subsequent infiltration of monocytes, macrophages and lymphocytes[57]. Du *et al.*[58] added that MCP-1 induces monocyte invasion into mesangium and vascular damage with increase production of ROS, metalloproteinases and proinflammatory mediators that worsen kidney injury and progression of DKD.

In this study the mean level of serum IL 6 showed significant rise in diabetic rats (subgroup IIA) as compared to control group. This increase confirms the previous explanation and was in accordance with Qi *et al.*[59] who declared that formation of MCP-1 by renal mesangial cells in response to hyperglycemia can lead to the accumulation and activation of mononuclear macrophages in the kidney as well as the secretion of a variety of growth factors and inflammatory transmitters.

In the current work, many ultrastructural changes were detected in the endothelial glomerular cells. Loss of endothelial fenestration was adopted by Finch *et al.*[60] who investigated the impact of diabetes on glomerular endothelial cell fenestrae in human and mouse kidney. They postulated that loss of fenestration could be attributed to decreased expression of Eps Homology Domain 3 (EHD3) proteins, one of endosomal transport proteins in glomerular endothelial cells which lead to aberrant VEGF signaling. In addition, some lining endothelial cells appeared apoptotic with dark nucleus and detached from glomerular basement membrane. Previous studies[61-63] have shown that hyperglycemia induces these changes by different mechanisms. First; increase level of cleaved caspase-3 in glomerular endothelial cells in relation to high glucose level. Second; high glucose level inhibits of endothelial nitric oxide synthase (eNOS) and induction of endothelial oxidative damage. Lastly; increased expression of VEGF-A from injured podocytes induces caveolae formation and diaphragms on endothelial fenestrae leading to dysfunction of endothelial cells and their detachment from GBM.

Podocytes are essential in preserving the integrity and permeability of the glomerular filtration barrier[64]. DN subgroup showed irregularly spaced secondary processes of podocyte with areas of flattening and effacement. Gil *et al.*[65] attributed these changes to hyperglycemia that induces activation of transient receptor potential canonical 6 (TRPC6) calcium channel causing calcium influx into podocytes. Increased intracellular calcium results in reorganization of actin filaments, disruption of nephrin, slit diaphragm, zonula occludens-1 (ZO-1) and consequently secondary process effacement. Also, Rein and Bader[66] explained flattening and effacement of podocytes' secondary processes by local increase in Ang II and VEGF which suppress expression of nephrin.

Another ultrastructure finding concerning podocytes is their primary processes showed electron dense deposits. This is attributed to high level of IL-6 that cause change of fine actin stress fibers into thick bundles of cortical actin filaments that could act as a nidus for actin condensation with disruption of slit diaphragms[67]. Activation of endothelin receptors (ET-1) on podocyte also mediates calcium influx that leads to activation of NF-κB and β-catenin signaling pathways with subsequent rearrangement of actin filaments and podocyte injury[68].

Our results revealed changes in parietal cells of Bowman's capsule at light and electron microscopic examination. These findings could be attributed to high level of ROS which induce DNA damage, lipid peroxidation and protein damage in several renal cells[69]. Hyperglycemia could also induce hypertrophy, cell cycle arrest, vacuolar degeneration and apoptosis in parietal cells[70].

On microscopic examination, obliteration of Bowman's space with tuft adhesion between parietal cells and podocytes appeared. This could be due to glomerular expansions with structural contacts between intact podocytes and parietal cells inducing formation of tuft adhesions[71]. On the other hand, shrunken glomeruli with widening of Bowman's space in some renal corpuscles were noticed in DN animals. This can be attributed to structural damage of various cellular components by oxidative stress[34,49,72].

In addition, light microscopic examination of renal cortex revealed arteriolar hyalinization with eosinophilic acellular deposits and tunica media thickening. This finding could be due to intramural deposition of plasma proteins and lipids within the arteriolar wall[73].

In the present study increase level of MDA and lower level of TAC in the sera of rats in diabetic and recovery subgroups (IIA&B) were noticed. These changes were in accordance with Nasef and M Khateib[34] and Hosseinzadeh *et al.*[74] who postulated that accumulation of free radicals result in lipid peroxidation of membrane lipids associated with significant increase MDA. They added that impaired activities of antioxidant defense mechanisms lead to significant decrease in TAC level.

The renal histological findings in the current study went parallel with the serological results as they revealed significant rise in the levels of blood urea nitrogen and serum creatinine in subgroup IIA. These were in accordance with some researches[75,76] who postulated that disruption of GFB integrity due to mesangial cell proliferation, matrix expansion and thickening of GBM can result in a decreasing the glomerular filtration rate and also impairment of kidney functions.

Significant increase in urine protein was also found in DN subgroup. This may be explained by cell damage due to accumulation of ROS. Alomari *et al.*[29] and Moratal *et al.*[77] postulated that ROS stimulate angiotensin II (Ang II) synthesis that causes an increase in intraglomerular pressure and glomerular permeability resulting in glomerular hyperfiltration and proteinuria.

In the present study, kidneys of subgroup IIB (spontaneous recovery subgroup) showed no improvement in the histological, biochemical and morphometrical results but worsen signs of degeneration were noticed representing irreversibility of STZ induced diabetic nephropathy due to persistent damage of β-cells[78].

Parallel to our results, a recent rat study[79]demonstrated that retinal samples obtained 12 weeks after diabetes induction showed no improvement in histological results with worsening symptoms of degeneration in the retinas, indicating that STZ-induced diabetic retinopathy is irreversible.

The majority of currently available treatments aimed at people who have advanced stages of DN. To postpone or perhaps eliminate this essential complication, it is desirable to design methods that target early stages of DN. Stem cell therapy has become one of the most promising treatment options for DN thanks to the development of contemporary medical technology in the field of regenerative medicine[80,81].

In the current study, rats of subgroup IIC which received a single dose of BM-MSCs after induction of diabetic nephropathy, showed moderate improvement in both biochemical profile and microscopic examinations with restoration of the architecture of renal corpuscles as compared to the DN subgroup. These results are in line with those of Abdel Aziz *et al*.[82] who discovered that delivering MSCs to patients decreased serum urea and creatinine, enhanced kidney function, and retained normal renal histology. The exact mechanism of the therapeutic potential of BM-MSCs is still not fully understood. However, several researchers attributed their therapeutic potential to paracrine mechanism through secretion of several growth factors, cytokines and chemokines such as VEGF, basic fibroblast growth factor (b-FGF), monocyte-chemoattractant protein- 1and insulin growth factor-1 (IGF-1) and hence their ability to influence the local environment, activate endogenous progenitor cells, and modify immune response[83,84].

Ni *et al*.[85] demonstrated that bone marrow-derived cells can colonize afflicted glomerular endothelium, transform into endothelial cells, and contribute in angiogenesis and renewal of the highly specialized glomerular microvasculature. There is evidence also that when oxidant-damaged mesangial cells are cocultured with MSCs in an in *vitro* system, MSCs can be trans-differentiated into mesangial cells[86].

According to Gad *et al*.[87], and Almeida *et al*.[88], mesenchymal stem cells can improve the renal alterations in DN due to its anti-inflammatory effects. They postulated that MSCs secrete HGF that decrease expression of pro-inflammatory cytokines as TNF-α, IL-1β and IL-6, and enhance expression of anti-inflammatory IL-10 and VEGF. Moreover, MSCs can secrete prostaglandin E2 (PGE2) that induce transition of macrophage into M2 phenotypes, hence the inflammatory process is suppressed and insulin sensitivity improved[89]. Furthermore, B lymphocyte proliferation and antibody generation are both suppressed by MSC[90]. This was confirmed in our study by the significant reduction of serum IL-6 in this subgroup when compared to diabetic nephropathy subgroup.

Interestingly, in the current study, significant reduction in the area % of collagen deposition was detected in MSCs treated animals. MSCs have an antifibrotic effect through suppression of TGF-β signaling pathway and collagens type I and IV deposition[91]. MSCs could also up-regulate organ-protective Interleukin-10 (IL-10) which is an antifibrotic agent[92]. Some investigators[93] also studied attenuating mesangial growth after injection of umbilical cord mesenchymal stem cells (UC-MSCs) in diabetic mice that mimics the role of human MSCs in decreasing profibrotic molecule. In contrast, other investigators noticed that BM-MSCs had no effect on fibrosis reduction[94,95]. Carvalho *et al*.[96] experimented on liver tissue and discovered that fibrosis was not reduced. Pecanha *et al*[97] whom employed skeletal muscle tissue also had a large scar.

Another explanation of the potential therapeutic effect of BM-MSCs, is that they can ameliorate oxidative stress which is an important damaging mechanism for developing diabetic kidney disease. In *vitro*, MSC-derived isolated mitochondria increased the synthesis of mitochondrial SOD and Bcl-2 while inhibiting ROS generation[80,98]. These could explain significant reduction in serum MDA level and significant increase in serum TAC level in BM-MSCs treated group when compared to the diabetic nephropathy subgroup. In addition, MSCs have an angiogenic effect that could enhance renal vascular regeneration, and anti-apoptotic effect which enhance podocyte survival via production of trophic factors as epidermal growth factor (EGF), stimulation of expression of nephrin, podocin, synaptopodin and ZO-1[99]. These effects could improve diabetic induced podocytes injury.

In this context, BM-MSCs represent a good therapeutic strategy to alleviate diabetic kidney injury, but there are many challenges that limit their use. The source of MSCs could affect their proliferation capability and efficacy. Safety of transplantation, tumorigenic formation and senescence of stem cells are all challenging for using MSCs as therapy[100].

EVs have got attention for their potential value for treatment of various diseases including kidney diseases[101,102]. In comparison to their secreted cells, EVs are considered more stable, less immunogenic, easily modified and could be stored for long period. In addition, the small size of EVs allows better tissue penetration and lower risk of embolization with intravascular injection than cell injection. EVs are also non-replicating vesicles hence there is no tumorigenic potential associated with their use[103,104].

Rats of subgroup IID that received a single dose EVs after induction of diabetic nephropathy, revealed evident histological structure improvement of renal corpuscles that was confirmed with the biochemical and morphometric results.

These outcomes were in line with those of Ebrahim *et al*.[105], who discovered that exosomes significantly improved renal function and restored renal tissues

histologically. According to He *et al*[106], MSC-derived exosomes were exhibited to be involved in glucose homeostasis via autophagy-related AMP-activated protein kinase (AMPK) pathway suppression.

One of the pivot cargos of EVs is micro RNAs that promote a number of therapeutic outcomes. Mao *et al*.[107] and Peng *et al*.[108] stated that miRNA-let-7a could suppress oxidative stress and apoptosis in renal cells via reducing ubiquitin-specific protease 22 (USP22). Faruk *et al*.[109] also postulated that improvement of adrenal injury following fluoride consumption was attributed to suppression of oxidative stress by BM-MSCs-EVs. This was in accordance with our results that showed significant reduction in serum MDA and significant elevation of serum TAC as compared to the diabetic nephropathy subgroup.

Moreover, Xiang *et al*.[110] discovered that anti-inflammatory effect of EVs was due to miR-223 and miR-124-3p/Ern1 of EVs which upregulate anti-inflammatory cytokines as IL-10 and downregulate of proinflammatory mediators and adhesion molecules as IL-6 and TNF-α. In our work, this was proved by significant reduction of serum IL-6 in EVs-treated subgroup comparable to DN subgroup.

Furthermore, Liu and Holmes[111] attributed the anti- fibrotic effect of EVs to miRNA-222 that could decrease expression of fibronectin and collagen type I caused by autophagy suppression in hyperglycemic state. Interestingly, our research showed that subgroup IID had the control pattern of collagen deposition.

Eventually, large autophagolysosome detected in podocytes implies that exosomes can activate autophagy to protect renal function[112]. The stimulation of autophagy by MSC-derived exosomes was discovered to ameliorate insulin resistance and directly regulate glucose metabolism[101].

The kidney biomarkers have also improved, supporting the therapeutic efficacy in EVS in subgroup IID along with the improvement in the histological structure of kidney tissue. Blood urea nitrogen, serum creatinine and urine proteins were all considerably improved and returned to their control ranges according to comparable earlier studies[113].

CONCLUSION

EVs as a cell-free therapy offer a unique and promising therapeutic line to MSC transplantation in the management of diabetic kidney disease. It provides several advantages when compared to MSCs. However, several difficulties must be overcomed before the issue can be fully addressed.

To achieve the highest therapeutic potential, it is necessary to standardize a high-efficiency isolation approach and create a database of EVs absorption, distribution, metabolism, and excretion. Also, to discover the reno-protective mechanisms within the EVs, as well as their way of action, more research would be required.

CONFLICT OF INTERESTS

There are no conflicts of interest.

REFERENCES

1. Sun H, Saeedi P, Karuranga S, Pinkepank M, Ogurtsova K, Duncan BB, *et al*. IDF Diabetes Atlas: Global, regional and country-level diabetes prevalence estimates for 2021 and projections for 2045. Diabetes research and clinical practice 2022; 183:109119. https://doi.org/10.1016/j.diabres.2021.109119.

2. Zhang P, Li T, Wu X, Nice EC, Huang C, Zhang Y. Oxidative stress and diabetes: antioxidative strategies. Frontiers of medicine 2020;14(5):583-600. https://doi.org/10.1007/s11684-019-0729-1.

3. Oguntibeju OO. Type 2 diabetes mellitus, oxidative stress and inflammation: examining the links. International journal of physiology, pathophysiology and pharmacology 2019;11(3):45. ISSN:1944-8171

4. Khalid M, Petroianu G, Adem A. Advanced Glycation End Products and Diabetes Mellitus: Mechanisms and Perspectives. Biomolecules 2022;12(4):542. https://doi.org/10.3390/biom12040542.

5. Sagoo MK, Gnudi L. Diabetic nephropathy: an overview. Diabetic Nephropathy 2020:3-7. https://doi.org/10.1007/978-1-4939-9841-8_1.

6. Duan YR, Chen BP, Chen F, Yang SX, Zhu CY, Ma YL, *et al*. Exosomal microRNA-16-5p from human urine-derived stem cells ameliorates diabetic nephropathy through protection of podocyte. Journal of Cellular and Molecular Medicine 2021;25(23):10798-10813. https://doi.org/10.1111/jcmm.14558.

7. Gupta R, Woo K, Jeniann AY. Epidemiology of end-stage kidney disease. InSeminars in vascular surgery 2021; 34 (1): 71-78. https://doi.org/10.1053/j.semvascsurg.2021.02.010.

8. Fu R, Sekercioglu N, Berta W, Coyte PC. Cost-effectiveness of deceased-donor renal transplant versus dialysis to treat end-stage renal disease: a systematic review. Transplantation direct 2020; 6(2). doi:10.1097/TXD.0000000000000974.

9. Mesnard B, Leroy M, Hunter J, Kervella D, Timsit MO, Badet L, *et al*. Kidney transplantation from expanded criteria donors: an increased risk of urinary complications–the UriNary Complications Of Renal Transplant (UNyCORT) study. BJU international 2022; 129(2):225-233. https://doi.org/10.1111/bju.15509.

10. Liu D, Cheng F, Pan S, Liu Z. Stem cells: a potential treatment option for kidney diseases. Stem cell research & therapy 2020; 11(1):1-20. https://doi.org/10.1186/s13287-020-01751-2.

11. Kuntin D, Genever P. Mesenchymal stem cells from biology to therapy. Emerging Topics in Life Sciences 2021; 5(4):539-548. https://doi.org/10.1042/ETLS20200303.

12. Sharma A, Gupta S, Archana S, Verma RS. Emerging trends in mesenchymal stem cells applications for cardiac regenerative therapy: Current Status and Advances. Stem Cell Reviews and Reports 2022 :1-57. https://doi.org/10.1007/s12015-021-10314-8.

13. Choudhary P, Gupta A, Singh S. Therapeutic advancement in neuronal transdifferentiation of mesenchymal stromal cells for neurological disorders. Journal of Molecular Neuroscience 2021; 71(5):889-901. https://doi.org/10.1007/s12031-020-01714-5.

14. Hmadcha A, Martin-Montalvo A, Gauthier BR, Soria B, Capilla-Gonzalez V. Therapeutic potential of mesenchymal stem cells for cancer therapy. Frontiers in Bioengineering and Biotechnology 2020:43. https://doi.org/10.3389/fbioe.2020.00043.

15. Pittenger MF, Discher DE, Péault BM, Phinney DG, Hare JM, Caplan AI. Mesenchymal stem cell perspective: cell biology to clinical progress. NPJ Regenerative medicine 2019;4(1):1-5. https://doi.org/10.1038/s41536-019-0083-6.

16. Van Niel G, Carter DR, Clayton A, Lambert DW, Raposo G, Vader P. Challenges and directions in studying cell–cell communication by extracellular vesicles. Nature Reviews Molecular Cell Biology 2022; 23(5):369-382. https://doi.org/10.1038/s41580-022-00460-3.

17. Kang T, Atukorala I, Mathivanan S. Biogenesis of extracellular vesicles. InNew Frontiers: Extracellular Vesicles. Springer, Cham. 2021: 19-43. https://doi.org/10.1007/978-3-030-67171-6_2.

18. Negahdaripour M, Owji H, Eskandari S, Zamani M, Vakili B, Nezafat N. Small extracellular vesicles (sEVs): Discovery, functions, applications, detection methods and various engineered forms. Expert Opinion on Biological Therapy 2021; 21(3):371-394. https://doi.org/10.1080/14712598.2021.1825677.

19. Gurung S, Perocheau D, Touramanidou L, Baruteau J. The exosome journey: From biogenesis to uptake and intracellular signalling. Cell Communication and Signaling 2021;19(1):1-9. https://doi.org/10.1186/s12964-021-00730-1.

20. Gowen A, Shahjin F, Chand S, Odegaard KE, Yelamanchili SV. Mesenchymal stem cell-derived extracellular vesicles: challenges in clinical applications. Front Cell Dev Biol 2020;8(149):1-8. https://doi.org/10.3389/fcell.2020.00149

21. Li Y, Cheng Q, Hu G, Deng T, Wang Q, Zhou J, *et al*. Extracellular vesicles in mesenchymal stromal cells: a novel therapeutic strategy for stroke. Exp Ther Med 2018;15:4067–4079. https://doi.org/10.3892/etm.2018.5993.

22. Mohan A, Agarwal S, Clauss M, Britt NS, Dhillon NK. Extracellular vesicles: novel communicators in lung diseases. Respiratory Research 2020; 21(1):1-21. https://doi.org/10.1186/s12931-020-01423-y.

23. Yin L, Liu X, Shi Y, Ocansey DK, Hu Y, Li X, *et al*. Therapeutic advances of stem cell-derived extracellular vesicles in regenerative medicine. Cells 2020; 9(3):707. https://doi.org/10.3390/cells9030707.

24. Bernardi S, Balbi C. Extracellular vesicles: from biomarkers to therapeutic tools. Biology 2020;9(9):258. https://doi.org/10.3390/biology9090258.

25. Zakaria DM, Zahran NM, Arafa SA, Mehanna RA, Abdel-Moneim RA. Histological and physiological studies of the effect of bone marrow-derived mesenchymal stem cells on bleomycin induced lung fibrosis in adult albino rats. Tissue engineering and regenerative medicine 2021;18(1):127-141. https://doi.org/10.1007/s13770-020-00294-0.

26. Rostom DM, Attia N, Khalifa HM, Abou Nazel MW, El Sabaawy EA. The therapeutic potential of extracellular vesicles versus mesenchymal stem cells in liver damage. Tissue Eng Regen Med 2020; 17:537-552. https://doi.org/10.1007/s13770-020-00267-3.

27. Ibrahim HF, Safwat SH, Zeitoun TM, El Mulla KF, Medwar AY. The Therapeutic Potential of Amniotic Fluid-Derived Stem Cells on Busulfan-Induced Azoospermia in Adult Rats. Tissue Eng Regen Med 2021; 18 (2):279-295. https://doi.org/10.1007/s13770-020-00309-w.

28. González-Cubero E, González-Fernández ML, Gutiérrez-Velasco L, Navarro-Ramírez E, Villar-Suárez V. Isolation and characterization of exosomes from adipose tissue-derived mesenchymal stem cells. Journal of Anatomy 2021;238(5):1203-1217. https://doi.org/10.1111/joa.13365.

29. Alomari G, Al-Trad B, Hamdan S, Aljabali A, Al-Zoubi M, Bataineh N, *et al*. Gold nanoparticles attenuate albuminuria by inhibiting podocyte injury in a rat model of diabetic nephropathy. Drug Deliv Transl Res 2020;10 (1):216-226. https://doi.org/10.1007/s13346-019-00675-6.

30. Salem AM, Ragheb AS, Hegazy MG, Matboli M, Eissa S. Caffeic acid modulates miR-636 expression in diabetic nephropathy rats. Ind J Clin Biochem 2019;34 (3):296-303. https://doi.org/10.1007/s12291-018-0743-0.

31. Ibrahim AA-S, Morsy MM, Abouhashem SE, Aly O, Sabbah NA, Raafat N. Role of mesenchymal stem cells and their culture medium in alleviating kidney injury in rats diabetic nephropathy. Egypt J Med Hum Genet 2020; 21:1-13. https://doi.org/10.1186/s43042-020-00064-6.

32. Lin L, Lin H, Wang D, Bao Z, Cai H, Zhang X. Bone marrow mesenchymal stem cells ameliorated kidney fibrosis by attenuating TLR4/NF-κB in diabetic rats. Life Sci 2020; 262:118385. https://doi.org/10.1016/j.lfs.2020.118385.

33. Abbaszadeh H, Ghorbani F, Derakhshani M, Movassaghpour A, Yousefi M. Human umbilical cord mesenchymal stem cell-derived extracellular vesicles: A novel therapeutic paradigm. J Cell Physiol 2020; 235 (2):706-717. https://doi.org/10.1002/jcp.29004.

34. Nasef AN, M Khateib BR. Study the potential therapeutic effect of garden cress (Lepidium sativum) on nephropathy diabetic rats: biological and biochemical studies. Alex Sci Exch J 2021; 42 (2):263-272. https://dx.doi.org/10.21608/asejaiqjsae.2021.165932.

35. Lodhi AH, Fiaz-ud-Din Ahmad KF, Madni A. Role of Oxidative Stress and Reduced Endogenous Hydrogen Sulfide in Diabetic Nephropathy. Drug Des Devel Ther 2021;15:1031-1043. https://doi.org/10.2147/DDDT.S291591.

36. Sindhughosa DA, AAGMK P. The involvement of proinflammatory cytokines in diabetic nephropathy: Focus on interleukin 1 (IL-1), interleukin 6 (IL-6), and tumor necrosis factor-alpha (TNF-α) signaling mechanism. Bali Medical Journal 2017;201(6):1. doi:10.15562/bmj.v6i1.299.

37. Bancroft J and Layton C: The hematoxylin and eosin, connective and mesenchymal tissues with their stains. In: Suvarna S, Layton C and Bancroft J (eds). Bancroft's Theory and Practice of Histological Techniques. 7th ed. Churchill Livingstone. Philadelphia. 2013 : 173-212. ISBN: 978-0-7020-4226-3

38. Dykstra MJ. Specimen preparation. In: Michael JD, editor. A Manual of applied techniques for biological electron microscopy.4th ed. New York: Plenum Press; 2017: 1–18. ISBN-13 : 978-0306444494

39. Balkawade RS, Chen C, Crowley MR, Crossman DK, Clapp WL, Verlander JW, *et al.* Podocyte-specific expression of Cre recombinase promotes glomerular basement membrane thickening. Am J Physiol-Renal Physiol 2019; 316 (5):1026-1040. https://doi.org/10.1152/ajprenal.00359.2018.

40. Sorour H, Abd-Elgalil M. Mesenchymal Stem cells Ameliorate Diabetic Renocortical Changes In A Rat Model: Histological, Morphometrical And Biochemical Study. J Med Histol 2019; 3 (2):132-161. doi: 10.21608/jmh.2020.40093.1080.

41. Stehlik-Barry K, Babinec AJ. Data analysis with IBM SPSS statistics: Packt Publishing Ltd. (2017)

42. Chen J. Diabetic Kidney Disease: Scope of the Problem. Diabetes and Kidney Disease 2022:37-47. 42- https://doi.org/10.1007/978-3-030-86020-2_3.

43. Lovre D, Thethi TK. Natural Course (Stages/Evidence-Based Discussion). In Diabetes and Kidney Disease. Springer, Cham 2022:49-74. https://doi.org/10.1007/978-3-030-86020-2_4.

44. Giusti S, Batuman V. Kidney transplantation and kidney pancreas transplantation. In: Diabetes and Kidney Disease. 2nd ed. Springer, Cham 2022:417-29. https://doi.org/10.1007/978-3-030-86020-2.

45. Goyal SN, Reddy NM, Patil KR, Nakhate KT, Ojha S, Patil CR, *et al*. Challenges and issues with streptozotocin-induced diabetes–a clinically relevant animal model to understand the diabetes pathogenesis and evaluate therapeutics. Chemico-biological interactions 2016 ; 244:49-63. https://doi.org/10.1016/j.cbi.2015.11.032.

46. Zaky AS, Kandeil M, Abdel-Gabbar M, Fahmy EM, Almehmadi MM, Ali TM, *et al*. The Antidiabetic Effects and Modes of Action of the Balanites aegyptiaca Fruit and Seed Aqueous Extracts in NA/STZ-Induced Diabetic Rats. Pharmaceutics 2022 ;14(2):263. https://doi.org/10.3390/pharmaceutics14020263.

47. Retnaningtyas E, Susatia B, Arifah SN, Lestari SR. The improvement of insulin level after hydrogen-rich water therapy in streptozotocin-induced diabetic rats. Vet World 2022; 15(1):182-187. doi: 10.14202/vetworld.2022.182-187.

48. Dariya B, Nagaraju GP. Advanced glycation end products in diabetes, cancer and phytochemical therapy. Drug Discovery Today 2020; 25(9):1614-1623. https://doi.org/10.1016/j.drudis.2020.07.003.

49. Santos HO, Penha-Silva N. Translating the advanced glycation end products (AGEs) knowledge into real-world nutrition strategies. European Journal of Clinical Nutrition 2021:1-7. https://doi.org/10.1038/s41430-021-01028-8.

50. Huang KP, Chen C, Hao J, Huang JY, Liu PQ, Huang HQ. AGEs-RAGE system down-regulates Sirt1 through the ubiquitin-proteasome pathway to promote FN and TGF-β1 expression in male rat glomerular mesangial cells. Endocrinology 2015 ; 156(1):268-279. https://doi.org/10.1210/en.2014-1381.

51. Bahreini E, Rezaei-Chianeh Y, Nabi-Afjadi M. Molecular mechanisms involved in intrarenal renin-angiotensin and alternative pathways in diabetic nephropathy-a review. Review of Diabetic Studies 2021; 17(1):1-10. https://doi.org/10.1900/RDS.2021.17.1.

52. Moratal C, Laurain A, Naïmi M, Florin T, Esnault V, Neels JG, *et al*. Regulation of Monocytes/Macrophages by the Renin–Angiotensin System in Diabetic Nephropathy: State of the Art and Results of a Pilot Study. International Journal of Molecular Sciences 2021; 22(11):6009. https://doi.org/10.3390/ijms22116009.

53. Aghadavoud E, Nasri H, Amiri M. Molecular signaling pathways of diabetic kidney disease; new concepts. Journal of Preventive Epidemiology 2017 ; 2(2):e09-.

54. Babel RA, Dandekar MP. A review on cellular and molecular mechanisms linked to the development of diabetes complications. Current Diabetes Reviews 2021; 17(4):457-473. https://doi.org/10.2174/157339 9816666201103143818.

55. Gonzalez CD, Carro Negueruela MP, Nicora Santamarina C, Resnik R, Vaccaro MI. Autophagy dysregulation in diabetic kidney disease: from pathophysiology to pharmacological interventions. Cells 2021; 10(9):2497. https://doi.org/10.3390/cells10092497.

56. Koch EA, Nakhoul R, Nakhoul F, Nakhoul N. Autophagy in diabetic nephropathy: a review. International urology and nephrology 2020; 52(9):1705-12. https://doi.org/10.1007/s11255-020-02545-4.

57. Li Y, Hou JG, Liu Z, Gong XJ, Hu JN, Wang YP, *et al*. Alleviative effects of 20 (R)-Rg3 on HFD/STZ-induced diabetic nephropathy via MAPK/NF-κB signaling pathways in C57BL/6 mice. Journal of Ethnopharmacology 2021; 267:113500. https://doi.org/10.1016/j.jep.2020.113500.

58. Du Q, Fu YX, Shu AM, Lv X, Chen YP, Gao YY, *et al*. Loganin alleviates macrophage infiltration and activation by inhibiting the MCP-1/CCR2 axis in diabetic nephropathy. Life Sciences 2021; 272:118808. https://doi.org/10.1016/j.lfs.2020.118808.

59. Qi SS, Shao ML, Ze S, Zheng HX. Salidroside from Rhodiola rosea L. attenuates diabetic nephropathy in STZ induced diabetic rats via anti-oxidative stress, anti-inflammation, and inhibiting TGF-β1/Smad pathway. Journal of Functional Foods 2021; 77:104329. https://doi.org/10.1016/j.jff.2020.104329.

60. Finch NC, Fawaz SS, Neal CR, Butler MJ, Lee VK, Salmon AJ, *et al*. Reduced glomerular filtration in diabetes is attributable to loss of density and increased resistance of glomerular endothelial cell fenestrations. Journal of the American Society of Nephrology 2022;33(6):1120-1136. doi: 10.1681/ASN.2021030294.

61. Bammert TD, Hijmans JG, Reiakvam WR, Ma'ayan VL, Brewster LM, Goldthwaite ZA, *et al*. High glucose derived endothelial microparticles increase active caspase-3 and reduce microRNA-Let-7a expression in endothelial cells. Biochemical and biophysical research communications 2017; 493(2):1026-1029. https://doi.org/10.1016/j.bbrc.2017.09.098.

62. Chen Y, Zhou B, Yu Z, Yuan P, Sun T, Gong J, *et al*. Baicalein alleviates erectile dysfunction associated with streptozotocin-induced type I diabetes by ameliorating endothelial nitric oxide synthase dysfunction, inhibiting oxidative stress and fibrosis. The Journal of Sexual Medicine 2020;17(8):1434-1447. https://doi.org/10.1016/j.jsxm.2020.04.390.

63. Locatelli M, Zoja C, Conti S, Cerullo D, Corna D, Rottoli D, *et al*. Empagliflozin protects glomerular endothelial cell architecture in experimental diabetes through the VEGF-A/caveolin-1/PV-1 signaling pathway. The Journal of Pathology 2022; 256(4):468-479. https://doi.org/10.1002/path.5862

64. Daehn IS, Duffield JS. The glomerular filtration barrier: a structural target for novel kidney therapies. Nat Rev Drug Discov 2021; 20(10):770-788. https://doi.org/10.1038/s41573-021-00242-0.

65. Gil CL, Hooker E, Larrivée B. Diabetic kidney disease, endothelial damage, and podocyte-endothelial crosstalk. Kidney Med 2021; 3(1):105-115. https://doi.org/10.1016/j.xkme.2020.10.005.

66. Rein J, Bader M. Renin-angiotensin system in diabetes. Protein and peptide letters 2017; 24(9):833-840. https://doi.org/10.2174/092986652466611707281 44357.

67. Srivastava T, Joshi T, Heruth DP, *et al*. A mouse model of prenatal exposure to Interleukin-6 to study the developmental origin of health and disease. Sci Rep 2021; 11(1):1-19. https://doi.org/10.1038/s41598-021-92751-6.

68. Sipovsky V, Smirnov A. Ultrastructural study of podocyte alterations in podocytopathies. Ann Rom Soc Cell Biol 2021; 25(2):1842-1850. ISSN:1583-6258

69. Zhong Y, Luo R, Liu Q, Zhu J, Lei M, Liang X, *et al*. Jujuboside A ameliorates high fat diet and streptozotocin induced diabetic nephropathy via suppressing oxidative stress, apoptosis, and enhancing autophagy. Food and Chemical Toxicology 2022; 159:112697. https://doi.org/10.1016/j.fct.2021.112697.

70. Kawaguchi T, Hasegawa K, Yasuda I, Muraoka H, Umino H, Tokuyama H, *et al*. Diabetic condition induces hypertrophy and vacuolization in glomerular parietal epithelial cells. Scientific reports 2021; 11(1):1-2.https://doi.org/10.1038/s41598-021-81027-8.

71. AL Tamimi JZ, AlFaris NA, Al-Farga AM, Alshammari GM, BinMowyna MN, Yahya MA. Curcumin reverses diabetic nephropathy in streptozotocin-induced diabetes in rats by inhibition of PKCβ/p66Shc axis and activation of FOXO-3a. The Journal of nutritional biochemistry 2021;87:108515. https://doi.org/10.1016/j.jnutbio.2020.108515.

72. Ragab R, El-Habiby MM, El-mehi A, Faried M. The protective effect of anise, insulin, and their combination in the nephropathy of diabetic rat model. Egyptian Journal of Histology 2021; 44(2):503-519. doi: 10.21608/EJH.2020.38032.1341

73. Herrera GA, Pozo-Yauner LD, Aufman JJ, Turbat-Herrera EA. Pathogenesis: Structural Changes in the Kidneys in Type 1 and Type 2 Diabetes. InDiabetes and Kidney Disease. Springer, Cham 2022: 105-154.

74. Hosseinzadeh A, Jani AM, Karimi MY, Siahpoosh A, Goudarzi M, Malayeri A. Evaluating the effect of hydro-alcoholic extract of Phoenix dactylifera L. spathe on streptozotocin-induced diabetic rats. Comparative Clinical Pathology 2021; 30(2):163-171. DOI:10.1007/s00580-021-03221-4

75. Ambalavanan R, John AD, Selvaraj AD. Nephroprotective role of nanoencapsulated Tinospora cordifolia (Willd.) using polylactic acid nanoparticles in streptozotocin-induced diabetic nephropathy rats. IET nanobiotechnology 2021; 15(4):411-417. https://doi.org/10.1049/nbt2.12030

76. Barutta F, Bellini S, Gruden G. Mechanisms of podocyte injury and implications for diabetic nephropathy. Clinical Science 2022; 136(7):493-520. https://doi.org/10.1042/CS20210625

77. Moratal C, Laurain A, Naïmi M, Florin T, Esnault V, Neels JG, *et al*. Regulation of Monocytes/Macrophages by the Renin–Angiotensin System in Diabetic Nephropathy: State of the Art and Results of a Pilot Study. International Journal of Molecular Sciences 2021; 22(11):6009. https://doi.org/10.3390/ijms22116009

78. Yang QH, Zhang Y, Jiang J, Wu MM, Han Q, Bo QY, *et al*. Protective effects of a novel drug RC28-E blocking both VEGF and FGF2 on early diabetic rat retina. International Journal of Ophthalmology 2018;11(6):935. https://doi.org/10.18240%2Fijo.2018.06.07

79. El-Halim A. The Possible Therapeutic Effect of Mesenchymal Stem Cells and their Exosomes on Experimentally Induced Diabetic Retinopathy in Rats: Histological and Immunohistochemical Study. Egyptian Journal of Histology 2020; 43(2):390-411. https://dx.doi.org/10.21608/ejh.2019.18175.1185

80. Wu Y, Zhang C, Guo R, Wu D, Shi J, Li L, *et al*. Mesenchymal stem cells: an overview of their potential in cell-based therapy for diabetic nephropathy. Stem Cells International 2021 ; 2021(6620811):1-12. DOI:10.1155/2021/6620811

81. Wang Y, Shan SK, Guo B, Li F, Zheng MH, Lei LM, *et al*. The Multi-Therapeutic Role of MSCs in Diabetic Nephropathy. Frontiers in Endocrinology 2021:678. https://doi.org/10.3389/fendo.2021.671566

82. Abdel Aziz MT, Abdel Wassef M, Ahmed HH, Rashed L, Mahfouz S , Aly MI, *et al*. The role of bone marrow derived- mesenchymal stem cells in attenuation of kidney function in rats with diabetic nephropathy. Diabetology& Metabolic Syndrome 2014; 6(34):1-10. https://doi.org/10.1186/1758-5996-6-34

83. Sun H, Pratt RE, Hodgkinson CP, Dzau VJ. Sequential paracrine mechanisms are necessary for the therapeutic benefits of stem cell therapy. American Journal of Physiology-Cell Physiology 2020;319(6):C1141-50. https://doi.org/10.1152/ajpcell.00516.2019

84. Chang D, Fan T, Gao S, Jin Y, Zhang M, Ono M. Application of mesenchymal stem cell sheet to treatment of ischemic heart disease. Stem Cell Research & Therapy 2021;12(1):1-0. https://doi.org/10.1186/s13287-021-02451-1

85. Ni W, Fang Y, Xie L, Liu X, Shan W, Zeng R, *et al*. Adipose derived mesenchymal stem cells transplantation alleviates renal injury in streptozotocin-induced diabetic nephropathy. .J Histochem Cytochem 2015; 63(11):842–853. https://doi.org/10.1369/0022155415599039

86. Wong CY, Tan EL, Cheong SK. In *vitro* differentiation of mesenchymal stem cells into mesangial cells when co-cultured with injured mesangial cells. Cell biology international 2014; 38(4):497-501. https://doi.org/10.1002/cbin.10231

87. Gad ES, Salama AA, El-Shafie MF, Arafa HM, Abdelsalam RM, Khattab M. The anti-fibrotic and anti-inflammatory potential of bone marrow–derived mesenchymal stem cells and nintedanib in bleomycin-induced lung fibrosis in rats. Inflammation 2020; 43(1):123-134. https://doi.org/10.1007/s10753-019-01101-2

88. Almeida A, Lira R, Oliveira M, Martins M, Azevedo Y, Silva K, *et al*. Bone marrow-derived mesenchymal stem cells transplantation ameliorates renal injury through anti-fibrotic and anti-inflammatory effects in chronic experimental renovascular disease. Biomedical Journal 2021. https://doi.org/10.1016/j.bj.2021.07.009

89. Khalil MR, El-Demerdash RS, Elminshawy HH, Mehanna ET, Mesbah NM, Abo-Elmatty DM. Therapeutic effect of bone marrow mesenchymal stem cells in a rat model of carbon tetrachloride induced liver fibrosis. Biomedical journal 2021; 44(5):598-610. https://doi.org/10.1016/j.bj.2020.04.011

90. Rivera-Cruz CM, Shearer JJ, Figueiredo Neto M, Figueiredo ML. The immunomodulatory effects of mesenchymal stem cell polarization within the tumor microenvironment niche. Stem cells international 2017; 2017. https://doi.org/10.1155/2017/4015039

91. Franco ML, Beyerstedt S, Rangel ÉB. Klotho and mesenchymal stem cells: a review on cell and gene therapy for chronic kidney disease and acute kidney disease. Pharmaceutics 2022;14(11):1-42. https://doi.org/10.3390/pharmaceutics14010011

92. Li H, Rong P, Ma X, Nie W, Chen C, Yang C, *et al*. Paracrine effect of mesenchymal stem cell as a novel therapeutic strategy for diabetic nephropathy. Life sciences 2018; 215:113-118. https://doi.org/10.1016/j.lfs.2018.11.001

93. Maldonado M, Huang T, Yang L, Xu L, Ma L. Human umbilical cord Wharton jelly cells promote extra-pancreatic insulin formation and repair of renal damage in STZ-induced diabetic mice. Cell Communication and Signaling 2017;15(1):1-3. DOI 10.1186/s12964-017-0199-5

94. Quintanilha LF, Mannheimer EG, Carvalho AB, Paredes BD, Dias JV, Almeida AS, *et al*. Bone marrow cell transplant does not prevent or reverse murine liver cirrhosis. Cell Transplant 2008;17(8):943–953. https://doi.org/10.3727/096368908786576453

95. Andrade BM, Baldanza MR, Ribeiro KC, Porto A, Pecanha R, Fortes FS, *et al*. Bone marrow mesenchymal cells improve muscle function in a skeletal muscle re-injury model. PLoS One 2015; 10(6):e0127561. https://doi.org/10.1371/journal.pone.0127561

96. Carvalho AB, Quintanilha LF, Dias JV, ParedesBD, Mannheimer EG, Carvalho FG, *et al*. Bone marrow multipotent mesenchymal stromal cells do not reduce fibrosis or improve function in a rat model of severe chronic liver injury. Stem Cells Dayt Ohio 2008; 26(5):1307–1314. https://doi.org/10.1634/stemcells.2007-0941

97. Peçanha R, Bagno L de LES, Ribeiro MB, Robottom Ferreira AB, Moraes MO, Zapata-Sudo G, *et al*. Adipose-derived stem-cell treatment of skeletal muscle injury. J Bone Joint Surg Am 2012 ;94(7):609–617. DOI: 10.2106/JBJS.K.00351

98. Konari N, Nagaishi K, Kikuchi S, Fujimiya M. Mitochondria transfer from mesenchymal stem cells structurally and functionally repairs renal proximal tubular epithelial cells in diabetic nephropathy in *vivo*. Scientific reports 2019; 9(1):1-4. https://doi.org/10.1038/s41598-019-40163-y

99. Wang Y, Liu J, Zhang Q, Wang W, Liu Q, Liu S, *et al*. Human umbilical cord mesenchymal stem cells attenuate podocyte injury under high glucose via TLR2 and TLR4 signaling. Diabetes Research and Clinical Practice 2021; 173:108702. https://doi.org/10.1016/j.diabres.2021.108702

100. Veceric-Haler Z, Cerar A, Perse M. (Mesenchymal) stem cell-based therapy in cisplatin-induced acute kidney injury animal model: risk of immunogenicity and tumorigenicity. Stem Cells International 2017; 2017. https://doi.org/10.1155/2017/7304643

101. Huang W, Zhu XY, Lerman A, Lerman L. Extracellular Vesicles as Theranostic Tools in Kidney Disease. Clinical Journal of the American Society of Nephrology 2022 ; 17(5):1-10. DOI: 10.2215/CJN.16751221

102. Eirin A, Lerman LO. Mesenchymal stem/stromal cell–derived extracellular vesicles for chronic kidney disease: are we there yet? Hypertension 2021; 78(2):261-269. https://doi.org/10.1161/hypertensionaha.121.14596

103. Nam GH, Choi Y, Kim GB, Kim S, Kim SA, Kim IS. Emerging prospects of exosomes for cancer treatment: from conventional therapy to immunotherapy. Advanced Materials 2020; 32(51):2002440. https://doi.org/10.1002/adma.202002440

104. Li S, Yi M, Dong B, Tan X, Luo S, Wu K. The role of exosomes in liquid biopsy for cancer diagnosis and prognosis prediction. International journal of cancer 2021; 148(11):2640-2651. https://doi.org/10.1002/ijc.33386

105. Ebrahim N, Ahmed IA, Hussien NI, Dessouky AA, Farid AS, Elshazly AM, *et al*. Mesenchymal stem cell-derived exosomes ameliorated diabetic nephropathy by autophagy induction through the mTOR signaling pathway. Cells 2018; 7(12):226. https://doi.org/10.3390/cells7120226

106. He Q, Wang L, Zhao R, Yan F, Sha S, Cui C, *et al*. Mesenchymal stem cell-derived exosomes exert ameliorative effects in type 2 diabetes by improving hepatic glucose and lipid metabolism via enhancing autophagy. Stem cell research and therapy 2020; 11(1):1-4. https://doi.org/10.3389/fendo.2021.780974

107. Mao R, Shen J, Hu X. BMSCs-derived exosomal microRNA-let-7a plays a protective role in diabetic nephropathy via inhibition of USP22 expression. Life Sci 2021; 268(118937):1-9. https://doi.org/10.3389/fendo.2022.1027686

108. Peng L, Chen Y, Shi S, Wen H. Stem cell-derived and circulating exosomal microRNAs as new potential tools for diabetic nephropathy management. Stem Cell Res Ther 2022; 13(1):1-19. DOI:10.1186/s13287-021-02696-w

109. Faruk EM, Alasmari WA, Fouad H, Nafea OE, Hasan RA. Extracellular vesicles derived from bone marrow mesenchymal stem cells repair functional and structural rat adrenal gland damage induced by fluoride. Life Sciences 2021; 270:119122. https://doi.org/10.1016/j.lfs.2021.119122

110. Xiang E, Han B, Zhang Q, Rao W, Wang Z, Chang C, *et al*. Human Umbilical Cord-Derived Mesenchymal Stem Cells Prevent the Progression of Early Diabetic Nephropathy Through Inhibiting Inflammation and Fibrosis. Stem Cell Res Ther 2020; 11:336. DOI:10.1186/s13287-020-01852-y

111. Liu Y, Holmes C. Tissue regeneration capacity of extracellular vesicles isolated from bone marrow-derived and adipose-derived mesenchymal stromal/stem cells. Front Cell Dev Biol 2021; 9(648098):1-12. https://doi.org/10.3389/fcell.2021.648098

112. Jin J, Shi Y, Gong J, Zhao L, Li Y, He Q, *et al*. Exosome secreted from adipose-derived stem cells attenuates diabetic nephropathy by promoting autophagy flux and inhibiting apoptosis in podocyte. Stem cell research & therapy 2019; 10(1):1-5. https://doi.org/10.1186%2Fs13287-019-1177-1

113. Wang S, Bao L, Fu W, Deng L, Ran J. Protective effect of exosomes derived from bone marrow mesenchymal stem cells on rats with diabetic nephropathy and its possible mechanism. American Journal of Translational Research 2021; 13(6):6423.

الملخص العربى

دراسة مقارنة لتأثير الخلايا الجذعية الوسطية للنخاع العظمى مقابل حويصلاتهم المفرزة علي الكريات الكلوية فى اعتلال الكلية السكرى فى الجرذان

إيمان مجدى محمد موسى، إنعام فيليب قلادة، صافيناز حسين صفوت، سيلفيا كميل صديق ساويرس

قسم الهستولوجيا وبيولوجيا الخلية ـ كلية الطب ـ جامعة الإسكندرية

المقدمة: يعد اعتلال الكلية السكرى واحدة من أكثر نتائج الأوعية الدموية الدقيقة انتشارا لمرض السكرى التى تؤدى إلى المراحل النهائيه لمرض الكلى. أصبح العلاج بالخلايا الجذعية الوسطية المشتقة من النخاع العظمى وحويصلاتها المفرزة خارج الخلية بروتوكول علاج محتمل لاعتلال الكلية السكرى.

الهدف: لمقارنة التأثير العلاجى المحتمل للخلايا الجذعية الوسطية المشتقة من النخاع العظمى والحويصلات المفرزة خارج الخلية على اعتلال الكلية السكرى المستحث فى الجرذان.

مواد وطرق البحث: تم استخدام أربعة ذكور جرذان بيضاء صغيرة فى عزل الخلايا الجذعية الوسطية المشتقة من النخاع العظمى والحويصلات المفرزة خارج الخلية. تم تقسييم اثنين وأربعين من ذكور الجرذان البيضاء البالغة على النحو التالى: المجموعة الأولى (المجموعات الظابطة): ١٨ جرذا. المجموعة الثانية (المجموعات المعالجة): ٢٤ جرذا، تلقى كل فأر حقنة واحدة داخل التجويف البريتونى من الأستريبتوزوتسين (٥٥ مجم / كجم من وزن الجسم). بعد التأكد من اصابتهم بالسكرى (معدل السكر فى الدم > ٢٥٠ مجم / ديسيلتر) ، تم تقسيمهم بالتساوى إلى المجموعة الفرعية الثانية أ (المجموعة الفرعية لاعتلال الكلية السكرى)، المجموعة الفرعية الثانية ب (المجموعة الفرعية للتعافى التلقائى)، المجموعة الفرعية الثانية ج (المجموعة الفرعية المعالجة بالخلايا الجذعية الوسطية المشتقة من النخاع العظمى) و المجموعة الفرعية الثانية د (المجموعة الفرعية المعالجة بالحويصلات المفرزه خارج الخلية). فى نهاية التجربة، تم جمع عينات الدم والبول للتحليل البيوكيميائى. كما تم استئصال الكلى ومعالجتها لدراستها بالميكرسكوب الضوئى و الإلكترونى والشكلى النسيجى القياسى. ثم خضعت البيانات المجمعة للتحليل الإحصائى.

النتائج: كشفت الدراسة الهستولوجية للمجموعة الفرعية لاعتلال الكلية السكرى عن عدم انتظام سمك الاغشيه الكبيبيه القاعديه و انفصال الخلايا البطانية المستماتة مع وجود فجوات بالخلايا الجدارية، كما تم طمس الأزرع الثانوية لكثير من الخلايا الرجلاء،و تسلل الخلايا الإلتهابية مع تكاثر خلايا المسراق وتوسع مطرس مسراق الكبيبة .و قد تم تأكيد هذه النتائج كيميائيا عن طريق زيادة ذات دلاله احصائيه فى متغيرات الكلى، علامات الأكسدة والإلتهاب وإنخفاض ذا دلاله احصائيه بعلامات مضادات الأكسدة. و ايضا أظهرت الدراسة الشكلية القياسية عن زيادة ذات دلاله احصائيه فى سمك الغشاء الكبيبى القاعدى و نسبة المساحة لألياف الكولاجين. هذا و قد خفف العلاج بالخلايا الجذعية الوسطية المشتقة من النخاع العظمى التغيرات الهستولوجية بالكريات الكلوية كما حسن من العلامات البيوكيميائية والتحليل الشكلى القياسى المستحث بمرض السكرى. وكشف إعطاء الحويصلات المفرزه خارج الخلية عن نتائج أفضل.

الإستنتاج: يمكن أن تكون الخلايا الجذعية الوسطية المشتقة من النخاع العظمى و الحوصيلات المفرزه خارج الخلايا مفيدة إلى حد كبير فى علاج اعتلال الكلية السكرى.مع الاخذ فى الاعتبار إن الحويصلات المفرزه خارج الخلية لديها طريقة علاجية واعدة مع آثار جانبية أقل عن الخلايا الجذعية الوسطية المزروعة .